A 3D Snapshot of Crustal Breakup Deduced From Seismic Analysis of the Tip of the NW South China Sea

P. Chao, G. Manatschal, P. Chenin, C. Zhang, J. Ren, X. Peng, J. Zheng

Tectonics®

RESEARCH ARTICLE
10.1029/2021TC007127

Key Points:

- We highlight for the first time the 3D crustal structure of the tip of the NW-South China Sea (NW-SCS) V-shaped basin
- Based on the architecture of sedimentary and magmatic deposits, we propose a 4D model for its breakup phase
- Proposition of a new retrograder breakup model for the NW-SCS

Correspondence to:

G. Manatschal,
manat@unistra.fr

Citation:

Chao, P., Manatschal, G., Chenin, P., Zhang, C., Ren, J., Peng, X., & Zheng, J. (2022). A 3D snapshot of crustal breakup deduced from seismic analysis of the tip of the NW South China Sea. *Tectonics*, *41*, e2021TC007127. https://doi.org/10.1029/2021TC007127

Received 28 OCT 2021
Accepted 10 MAY 2022

Author Contributions:

Conceptualization: P. Chao, G. Manatschal
Data curation: X. Peng, J. Zheng
Funding acquisition: G. Manatschal, J. Ren, X. Peng, J. Zheng
Investigation: P. Chao, G. Manatschal, P. Chenin
Methodology: P. Chao, G. Manatschal
Project Administration: G. Manatschal, P. Chenin, J. Ren, X. Peng, J. Zheng
Supervision: G. Manatschal, J. Ren, X. Peng
Writing – original draft: P. Chao, G. Manatschal, P. Chenin
Writing – review & editing: P. Chao, G. Manatschal, P. Chenin, C. Zhang

A 3D Snapshot of Crustal Breakup Deduced From Seismic Analysis of the Tip of the NW South China Sea

P. Chao[1,2], G. Manatschal[1], P. Chenin[1], C. Zhang[3], J. Ren[2,3], X. Peng[4], and J. Zheng[4]

[1]Université de Strasbourg, CNRS, ENGEES, ITES UMR 7063, Strasbourg, France, [2]College of Marine Science and Technology, China University of Geosciences, Wuhan, China, [3]Southern Marine Science and Engineering Guangdong Laboratory, Guangzhou, China, [4]CNOOC Ltd.-Shenzhen Branch, Shenzhen, China

Abstract Based on a high-resolution seismic reflection data set, we describe and map rift domains at the tip of the V-shaped NW-South China Sea (NW-SCS) Basin. We compare our rift domain map with seismic refraction, magnetic and gravity field data, and previously mapped Continent-Ocean Boundaries (COB). We also define and map syn-breakup sedimentary and magmatic sequences across the sediment-rich NW-SCS, which enables us to reconstruct the tectono-stratigraphic evolution of the area. This work enables us to describe and discuss the 3D architecture and nature of the crust at the tip of the NW-SCS, investigate how extensional and magmatic processes interacted during the breakup, and propose a kinematic model for late rifting, breakup, and finally stalling of the seafloor spreading system. This study provides exceptionally well-documented insights into the spatial and temporal evolution at the tip of a so-called "rift propagator," and enables us to show that breakup in the NW-SCS may rather correspond to a "retrograder," in which the extension zone retreats due to the reorganization of a failing rift system.

1. Introduction

The breaking up of continents and the formation of new oceanic crust is a crucial phase of plate tectonics. Unlike seafloor spreading or subduction, both of which are steady-state processes, the breakup is a transient event and is therefore rare and difficult to observe. There are only a handful of examples where the breakup stage is well documented, among which are the Woodlark basin (Taylor et al., 2009), the Gulf of California (Lizzaralde et al., 2007), the northern tip of the Red Sea (Ligi et al., 2018), and the Afar/western Gulf of Aden (Nonn et al., 2019). However, the magmatic budget, potential driving mechanisms, and kinematic settings are different among these examples and at present no universal model exists to explain how breakup propagates. Different models for rifting propagation were proposed by Courtillot (1982), Vink (1982), and Taylor et al. (2009), among others. These models concluded that the tip of a rift propagator is not an Eulerian pole, which is in line with numerical simulations proposed by Le Pourhiet et al. (2018) for the SCS. Nirrengarten et al. (2018) proposed a more complex rift propagator model for the southern North Atlantic, where the extension was simultaneously partitioned between different basins that formed ahead of a propagating lithospheric breakup. Luo et al. (2021) proposed a similar model for the SW-SCS (see their Figure 12c). This model is also supported by the studies of Le Pourhiet et al. (2017) and Neuharth et al. (2021), who showed, based on numerical modeling, that the linkage of rift segments can result in the formation of continental micro-blocks. While these models explain how rift propagators may develop, only the model of Le Pourhiet et al. (2018) tries to resolve why rift propagators in the SCS were not able to break through the continent and why they finally stalled. These authors suggested that the far-field compression due to the west-to-east topographic gradient across the Indochinese Peninsula prevented the propagation of lithospheric breakup. Two alternative explanations are: (a) the inherited magmatic arc-crust trending NE-SW ahead of the NW-SCS propagator was too strong to be rifted and inhibited a successful breakup (Chenin et al., 2015; Courtillot, 1982) and/or (b) slab-pull related to the subduction systems bounding the SCS to the south and to the east may have controlled the extensional kinematic setting in the SCS (Sibuet et al., 2016). One of the aims of the present study is to discuss why and when rift propagation failed, and how the strain was distributed during this failure in the NW-SCS.

Investigating the tip of the V-shaped NW-SCS Basin gives us the opportunity to look at a snapshot of a breakup system. Other advantages are the excellent seismic dataset available, the proximity of IODP drill holes (U1499, U1502; Sun et al., 2018), and the high sedimentation rates during the breakup, which provide an efficient recorder of the tectono-stratigraphic evolution. In addition, unlike many other distal hyperextended rifted margins (e.g.,

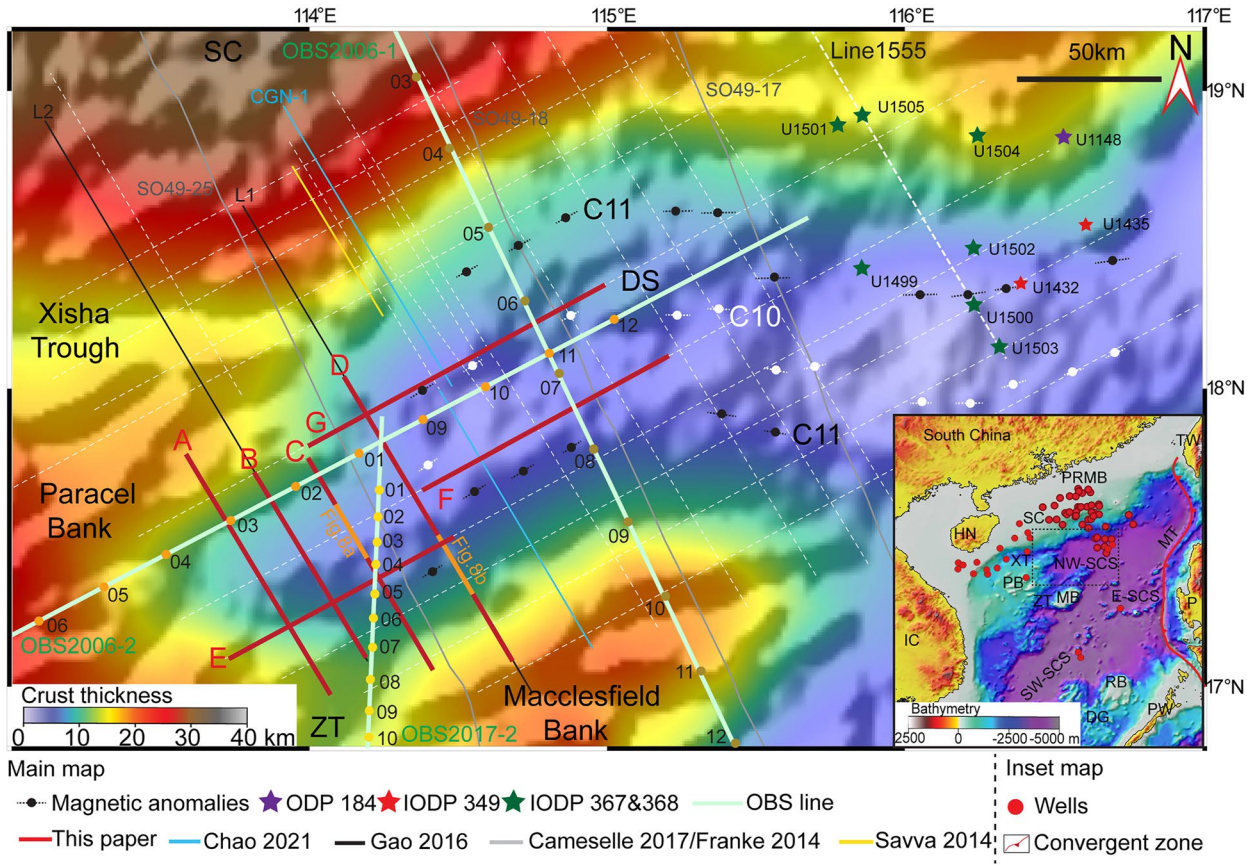

Figure 1. Location of the study area in the NW South China Sea and of the used datasets. Crustal thickness map based on gravity inversion with superimposed shaded relief free-air gravity anomaly from Gozzard et al. (2018). Inset in the right lower corner shows bathymetric map of the SCS. Location of the main seismic reflection lines (red lines) and refraction lines (pale green lines) presented in this paper. The locations of the IODP drill sites are based on Li et al. (2015) and Sun et al. (2018). The locations of the magnetic anomalies are based on Briais et al. (1993). The white dotted lines display the seismic reflection lines used in this research. The locations of wells are based on Gao et. (2016), Lei et al. (2020), Pang et al. (2018), Sun et. (2018), Zhang et al. (2019). Abbreviations used in the figure: DG, Dangerous Ground (Nansha); DS, Double-peak Seamount; E-SCS, East South China Sea; HN, Hainan; IC, Indochina; MB, Macclesfield Bank; MT, Manila Trench; NW-SCS, North West South China Sea; P, Philippines; PB, Paracel Bank (Xisha Islands); PRMB, Pearl River Mouth Basin; PW, Palawan; RB, Reed Bank (Liyue); SC, South China Continental Margin; SW-SCS, South West South China Sea; TW, Taiwan; ZT, Zhongsha Trough.

Rowan, 2018), the limited volume of magmatic additions and the lack of salt do not mask the stratigraphic record of the breakup process.

Of major importance is the recent study by Li et al. (2021) who investigated the crustal structure below the Zhongsha Block (Macclesfield Bank; Figure 1) and adjacent abyssal basins, complementing earlier work by Ding et al. (2012) and Wu et al. (2012). Based on seismic refraction studies, these authors proposed a crustal model for the NW-SCS that forms the foundation of the present study. Cameselle et al. (2017, 2020) and Franke et al. (2014) proposed seismic interpretations (for locations of their lines see Figure 1) that partially conflict with the interpretations by Ding et al. (2020), in particular about the structure of the ocean-continent transition (OCT). A detailed description of the OCT from the central N-SCS was proposed by Zhang, Sun, Manatschal, Pang, Li, et al. (2021) based on IODP drill hole data and seismic reflection lines located more than 250 km east of the area investigated in the present study. The OCT structure proposed by Zhang, Sun, Manastchal, Pang, Qiu, et al. (2021) compares well with the one we propose below.

The aim of the present study is twofold. First, we describe the 3D crustal architecture of the OCT and its along-strike variability; we map the distribution of rift domains and analyze the syn-rift sedimentary sequence at the tip of the NW-SCS. This allows us to propose a 3D crustal model for this V-shaped rift basin and to discuss how extensional and magmatic processes interacted and were recorded in the syn-rift sedimentary sequence.

Second, we correlate the syn-rift sedimentary sequences along strike, discuss how breakup evolved at the tip of the NW-SCS, and investigate the processes controlling whether a rift system goes breakup, reorganizes, or stalls.

2. Geological Setting

The SCS, the largest marginal sea in the western Pacific region, opened over the remnants of a convergent tectonic system. Indeed, the Mesozoic subduction of the paleo-Pacific plate beneath the South China Block (J. Li et al., 2014; Zhou et al., 1995, 2006) was associated with extension and magmatic activity in the hanging wall. A change in subduction polarity during the Late Cretaceous (Hall, 1996; Sun et al., 2006) led to multiphase rifting and crustal/lithospheric thinning (P. Li, 1993), and eventually resulted in the opening of two V-shaped basins, the older one in the NW and the younger one in the SW (Figure 1) (Taylor & Hayes, 1983). Thus, the western SCS formed over a complex basement including arc material and a subcontinental mantle that was likely depleted during the previous Mesozoic subduction (Pang et al., 2021; Sun et al., 2019; Zhang, Sun, Manastchal, Pang, Qiu, et al., 2021; Zhao et al., 2020).

In this study, we focus on the termination of the NW V-shaped basin, which separates the Western Pearl River Mouth Basin and China's continental margin in the north from the Macclesfield-Paracel Block (Zhongsha-Xisha) in the south (Figure 1). Cameselle et al. (2017, 2020) suggested that the spreading center propagated westwards and died shortly before reaching the Xisha Trough in the late Early Oligocene, an interpretation that is not compatible with the observations reported in the present study. Ding et al. (2012); Wu et al. (2012); Franke et al. (2014); Gao et al. (2016); Cameselle et al. (2017, 2020); Wang et al. (2020); and Chao et al. (2021) used different approaches to interpret the NW-SCS. As a result, they interpreted differently (a) magmatic budgets at breakup time, (b) distributions of the Continent Ocean Boundary (COB) or limits of the Ocean Continent Transition (OCT), and (c) details on how the breakup process was recorded in the study area. These aspects will be discussed in Section 5 of the present study.

The age of rifting onset in the NW-SCS is poorly constrained and usually reckoned to be 65 Ma, which corresponds to the stratigraphic marker horizon Tg (Xie et al. [2019]; for a review see also Chao et al. [2021]). Based on the occurrence of magnetic anomalies C11 and C10, Briais et al. (1993) and Gee et al. (2007) suggested that breakup occurred at ca. 30–28 Ma (late Early Oligocene). A key to understanding the characteristics of the breakup is to evaluate the tectono-magmatic evolution and its link to the OCT architecture. While Franke et al. (2014) proposed that the NW-SCS is a magma-poor rifted margin with possible exhumed mantle domains, Ding et al. (2020) showed that there is neither evidence for Seaward Dipping Reflections (SDR), nor for mantle exhumation. Based on these observations, Ding et al. (2020) classified the NW-SCS margin as an *intermediate margin*. This interpretation is in line with refraction data showing a high-velocity lower crust in the OCT (more than 7 km/s; Y. Li et al. [2021]), which suggests that breakup was controlled by magma. Further details on the breakup process were provided by Zhang, Sun, Manastchal, Pang, Li, et al. (2021); Zhang, Sun, Manastchal, Pang, Qiu, (2021) from the central N-SCS. These authors demonstrated, based on seismic reflection data and IODP 367/368 drill hole data, that the OCT includes hybrid crust (i.e., crust i.e., comprised of both extended pre-rift continental crust and newly formed magmatic crust), and that breakup was linked to interactions between detachment faulting and magmatic processes. These authors also constrained breakup to have occurred at anomaly C11 (about 30 Ma), in line with Nirrengarten et al. (2020). However, these studies are located more than 250 km east of the present study area. Since breakup is commonly considered to have propagated westward, its age might be younger than 30 Ma in the present study area. However, without drill hole calibration it is not possible to precisely determine the age of the breakup. In the present study, we base our ages on the occurrence of anomaly C10n in the study area, dated 28 Ma by Briais et al. (1993). However, magnetic anomalies are poorly identified in the NW sub-basin, and thus the exact age of breakup remains debated.

3. Data, Methods, and Terminology

3.1. Data Used and Acquisition Parameters

With the permission of the China National Offshore Oil Corporation (CNOOC), we had access to and interpreted a large, high-resolution seismic dataset, from which we selected seven seismic lines referred to as lines A to G (Figure 1). These multichannel seismic (MCS) sections, which record down to 12 s Two-Way Travel Time (TWT), belong to a large survey that imaged ca. 5,000 km of multichannel 2D sections covering the entire

NW-SCS sub-basin (approximately 35,000 km^2). NNW-SSE-oriented seismic lines have a spacing of 20 km and those oriented ENE-WSW a spacing of ca. 15 km. The seismic signal was generated using a Bolt Longlife Airgun (63 L) by means of compressed air (2,000 psi). Record length and sampling rate were set at 11,996 ms TWT and 2 ms, respectively. The acquired signals were recorded within 396 channels using a fold of 99 and lie in the frequency range of 40–60 Hz, allowing a vertical resolution up to 40 m. Data were processed through Omega V1.8.1 software, applying a bandpass filter (ranging from 6 Hz of low-cut frequency and 12 dB/s of low-cut slope to 136 Hz of high-cut frequency and 276 dB/s of high-cut slope), denoising and amplitude compensation and a post-stack time Kirchhoff migration (for more details see Chen et al. [2021]).

In order to compare our interpretation of seismic reflection data and to obtain further constraints on the nature of the crust in the study area, we include three seismic refraction lines (OBS2006-1 and OBS2006-2 published and described by Wu et al. (2012), and OBS2017-2 line published and described by Li et al. (2021); see Figure 1 for line locations).

The nearest drill holes penetrating the OCT are those from the International Ocean Discovery Program (IODP) Expeditions 367/368/368X (Larsen et al. [2018]; see Figure 1 for well locations). These drill sites, located approximately 300 km east of the study area, have been described by Zhang, Sun, Manastchal, Pang, Li, et al. (2021). We are aware that a precise stratigraphic correlation between our seismic sections and the IODP drill hole data is not possible due to the distance between the two sites. However, we consider that the time difference between the breakup event at the two sites is minor, which is supported by the fact that they contain magnetic anomalies of the same age (for more details see Chao et al. [2021]).

3.2. Methods

The present study is based on a careful analysis of high-resolution seismic reflection data from the tip of the NW-SCS, to describe the structures, magmatic additions, and sediment deposits formed during the breakup phase and deducing where, when, and how breakup occurred. Our seismic reflection interpretation aims to provide a coherent description of the geometrical relationships observed along the lines. For the seven seismic lines presented in this paper, we show separately the raw seismic section, its line drawing, and its interpretation in terms of sedimentary sequences. This enables the reader to comprehend and verify our observations and compare them with our interpretations. Our interpretation workflow is based on four successive steps, namely: (a) identification of first-order seismic interfaces (seafloor, top acoustic basement, Moho) and of rift domain boundaries; (b) definition of sedimentary sequences based on geometrical relationships between sediment reflections and top acoustic basement; (c) characterization of the nature of basement in the OCT, including a comparison with seismic refraction data; (d) mapping and description of faults, including fault offsets, sealing levels and terminations of reflectors. This approach allows us to build a coherent interpretation, in which first-order and most objective observations are established first, building the frame for subsequent, more subjective interpretations. The definition of sedimentary sequences allows us to build a relative temporal and spatial framework for the formation of the OCT at the tip of the NW-SCS.

3.3. Terminology and Definitions Used in This Study

3.3.1. Definition of First-Order Interfaces

In this study, we define the top of the acoustic basement (Tb) as a high-amplitude and well-imaged reflection corresponding to the interface between compactable sediments and the acoustic basement. Since the acoustic basement is partially made of highly metamorphosed pre-rift sediments emplaced during previous tectonic events, in our interpretation Tb represents an interface without any time or genetic connotation. Following Warner (1987), Moho is interpreted to occur in time sections at a constant two-way travel time, despite the highly variable structure of the overlying crust. The apparent flatness of seismic Moho also referred to as the "10 s rule", is an artifact produced when the crust is in local isostatic equilibrium. Because breakup in the NW-SCS occurred at ca. 28 Ma (Briais et al. [1993]; see also the previous section) thermal equilibrium has not been achieved yet, and thus seismic Moho lies typically between 8 and 9 s TWT (Chao et al., 2021).

Although both Tb and Moho represent physical interfaces that can be objectively imaged and observed, their nature is subject to geological interpretation, in particular in the OCT. In the NW-SCS, Tb corresponds either

to an initial, inherited contact between pre-rift sediments and continental crust, also referred to as Tg, which is the classical interpretation of Tb; or Tb can represent an exhumed fault or the top of a newly created magmatic crust. Similarly, the Moho can either represent an interface separating continental and mantle rocks (classical interpretation), correspond to a fault contact, represent an alteration front (e.g., serpentinization front beneath hyperextended crust or at exhumed mantle domains), or represent contact with newly formed igneous rocks. Note that, in the line drawings we consider Tb and Moho without any genetic connotation, while in the interpreted sections we provide a geological interpretation of the nature of both Tb and Moho.

3.3.2. Definition of Rift Domains and Domain Boundaries

In this contribution, we consider three main rift domains, namely continental, OCT, and oceanic. The definition of these domains relies mainly on crustal shapes (i.e., the outline formed by Tb and Moho), total accommodation space, and top basement topology (Tugend et al., 2014), all observable on seismic reflection sections. Even where Moho is not imaged, assuming the apparent flatness of the latter (e.g., "10 s rule" of Warner [1987]), first-order shapes (wedge-vs. box-shape) can be distinguished. The continental domain is characterized by a wedging crustal shape, a total accommodation space that is moderate compared to the other domains considered, and a faulted Tb. The oceanic domain is characterized by a box-shaped crust with a smooth Tb that is sub-horizontal and parallel to seismic Moho (when observed), where accommodation space is large and where sediments show only passive infill geometries. The domain in-between corresponds to the OCT domain. It is characterized by a faulted Tb dominated by magmatic additions and thus may display uneven topography. Its continent-ward limit is marked by a break in the slope or a lowering in the dip of Tb compared to the adjacent continental domain. The oceanward boundary of the OCT often corresponds to a basement high and is marked by a break in the slope of Tb, from continent-ward dipping to sub-horizontal in the adjacent oceanic domain (Chao et al., 2021).

Each of these domains is associated with a specific type of crust. On the one hand, the basement of the continental domain is entirely made of unequivocal continental crust. When the continental crust is less than 3 s TWT-thick, we refer to it as the hyperextended crust. On the other hand, the basement of the oceanic domain is made of unequivocal, Penrose-type oceanic crust. The basement of the OCT domain between them is more complex: while its continent-ward part may be comprised of hybrid crust, its oceanward part is made of highly faulted, but fully magmatic proto-oceanic crust.

3.3.3. Definition of Sedimentary Mega-Sequences, Faults, and Magmatic Additions

In this study, we define the sediment layer as the layer made of compactable sediments bounded by Tb and the seafloor. We distinguish between two mega-sequences, a syn-rift one and a post-rift one. We define the base of the syn-rift sedimentary mega-sequence as Tb, the interface that is capping the seismic basement. Its top is defined as the breakup interface (Bi), a surface that represents the lithospheric breakup time and that is approximated as an isochron in the limited-extent area of our study. Therefore, in our definition, the syn-rift mega-sequence includes the sediments deposited during the formation of the OCT domain, in other words during the breakup phase (cf. paragraph Definition of Breakup below). All sediments above Bi show passive infill and do not display evidence for significant tectonic overprint. Therefore, we define them as the post-rift mega-sequence.

Faults are not directly imaged by seismic methods; however, their existence can be deduced from offsets in Tb and/or in other interfaces/reflections. In this study, we identify the breakaways of high-angle normal faults and, wherever possible, syn-tectonic sedimentary- and/or magmatic sequences, as well as post-tectonic sequences that seal faults. Such observations enable us to determine relative fault ages. Where possible, we also define the levels where faults sole out at depth. These levels may correspond to brittle-ductile transitions (Sutra & Manatschal, 2012) or, alternatively, to the top of underplated material. In OCTs, magma emplacement, hydration, and the occurrence of extensional detachment systems result in a complexity that cannot be deduced from seismic observations alone. Although interpretations of faults and magmatic additions are non-unique, their interpretation should be coherent and fit with both geophysical and geological observations.

3.3.4. Definition of Breakup

The term breakup is here used to describe the transition from crustal separation, referred to as crustal breakup, to onset of steady-state seafloor spreading, referred to as lithospheric breakup. A breakup is thus a lasting event that is expressed by a transition zone (the OCT), rather than an instantaneous event that would correspond to a well-defined and mappable boundary (see also Chao et al. [2021]).

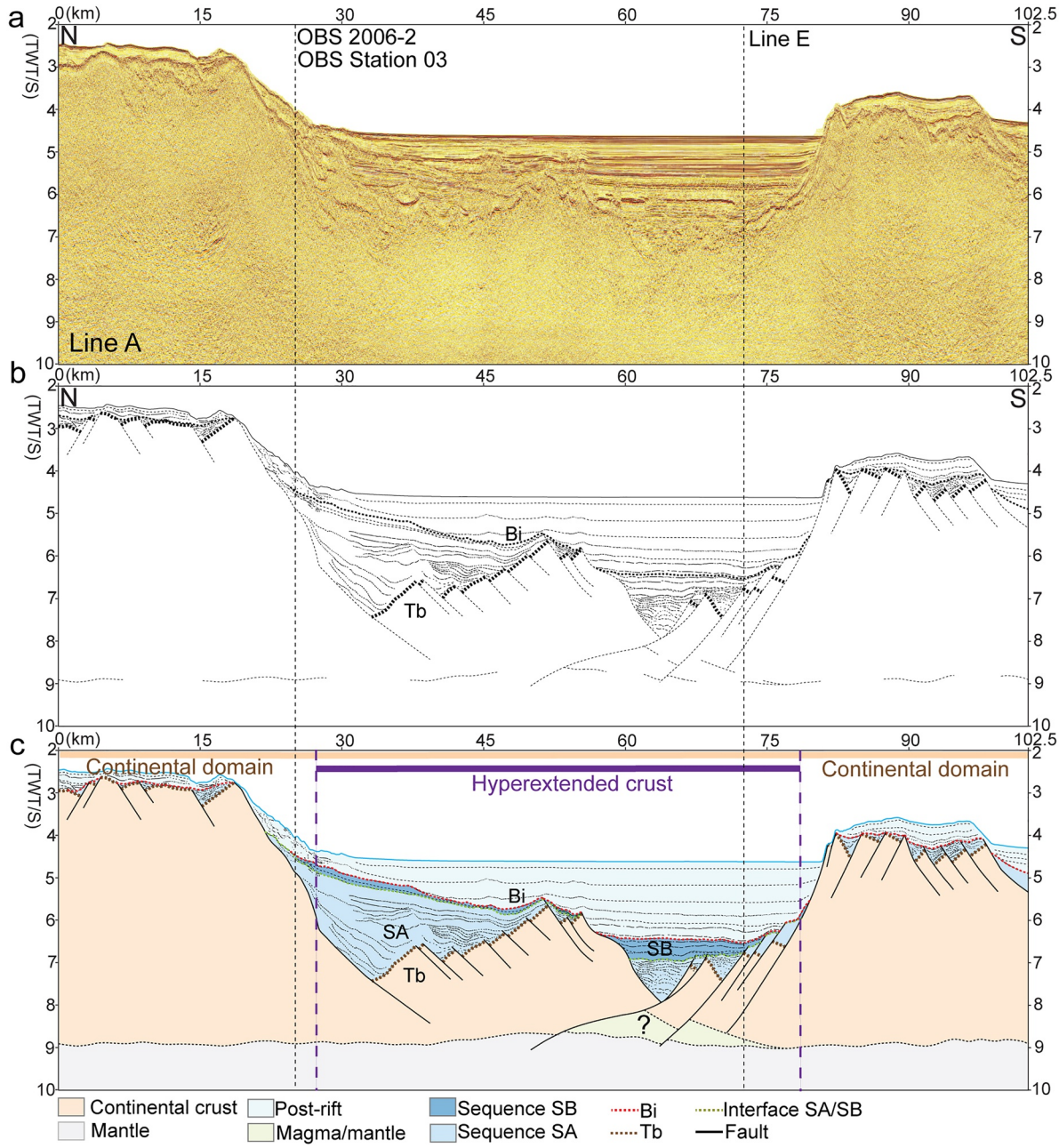

Figure 2. Seismic reflection section Line A across the tip of the propagator, for location see Figure 1. (a) Line A seismic reflection section in time with locations of cross lines (thin dashed lines). (b) Line drawing of Line A, the bold dashed lines are Tb and Bi. (c) Seismic interpretation of Line A with first-order interfaces, stratigraphic horizons and the tectonic structures. Three sedimentary sequences (SA, SB and post-rift) were defined (for explanation see discussion section). Abbreviations used in the figure: Bi, Breakup interface; Tb, Top acoustic Basement.

4. Seismic Reflection Lines: From Observations to Seismic Interpretations

4.1. First-Order Seismic Interfaces and Rift Domain Boundaries

In the present section, we define the main interfaces, that are, seafloor, top basement (Tb), and Moho, and distinguish between a continental domain that includes thinned continental crust and hyperextended crust (i.e., where crust is ≤3 s TWT), an OCT domain and an oceanic domain (for definitions see Section 3.3). We first only refer to the line drawings of Figures 2b–9b and will refer to and discuss the interpretations shown in Figures 2c–9c in later parts of this paper, when integrating second-order and more subjective observations and interpretations.

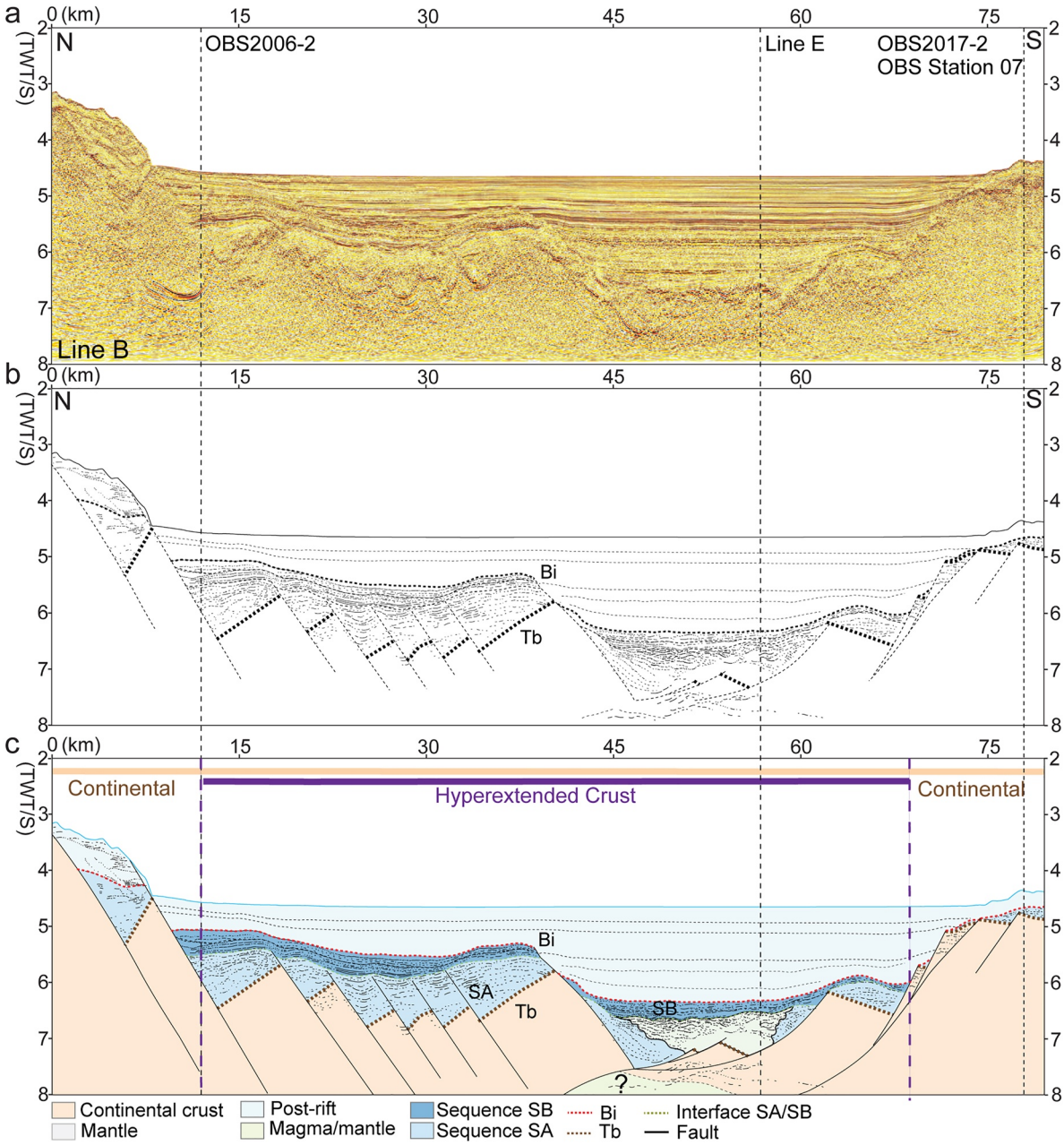

Figure 3. Seismic reflection section Line B across the tip of the propagator, for location see Figure 1. (a) Line B seismic reflection section in time with locations of cross lines (thin dashed lines). (b) Line drawing of Line B, the bold dashed lines are Tb and Bi. (c) Seismic interpretation of Line B with first-order interfaces, stratigraphic horizons, and tectonic structures. Three sedimentary sequences (SA, SB and post-rift) were defined (for explanation see discussion section). Abbreviations used in the figure: Bi, Breakup interface; Tb, Top acoustic Basement. Line B is the same line as seismic section L2, which has been published in Gao et al. (2016).

4.1.1. Line A

Line A (Figure 2a) is the westernmost section that images across the tip of the V-shaped basin (for location see Figure 1). The seafloor is slightly structured and lies at ca. 2.5 s TWT from km 0 to 17, and then deepens down to 4.5 s TWT. From km 30 to 80, the seafloor is flat, before it steps up and remains at ca. 3.5 s TWT. Seafloor steps down again at km 100 to 4 s TWT.

Tb is largely sub-horizontal and offset by only small normal faults from km 0 to 17 (Figure 2b). A major fault with an offset of ca. 4 s TWT separates the sub-horizontal Tb from a continent-ward tilted block that is offset by minor oceanward-dipping normal faults. Between km 55 and 65, Tb deepens abruptly down to 8 s TWT. In the

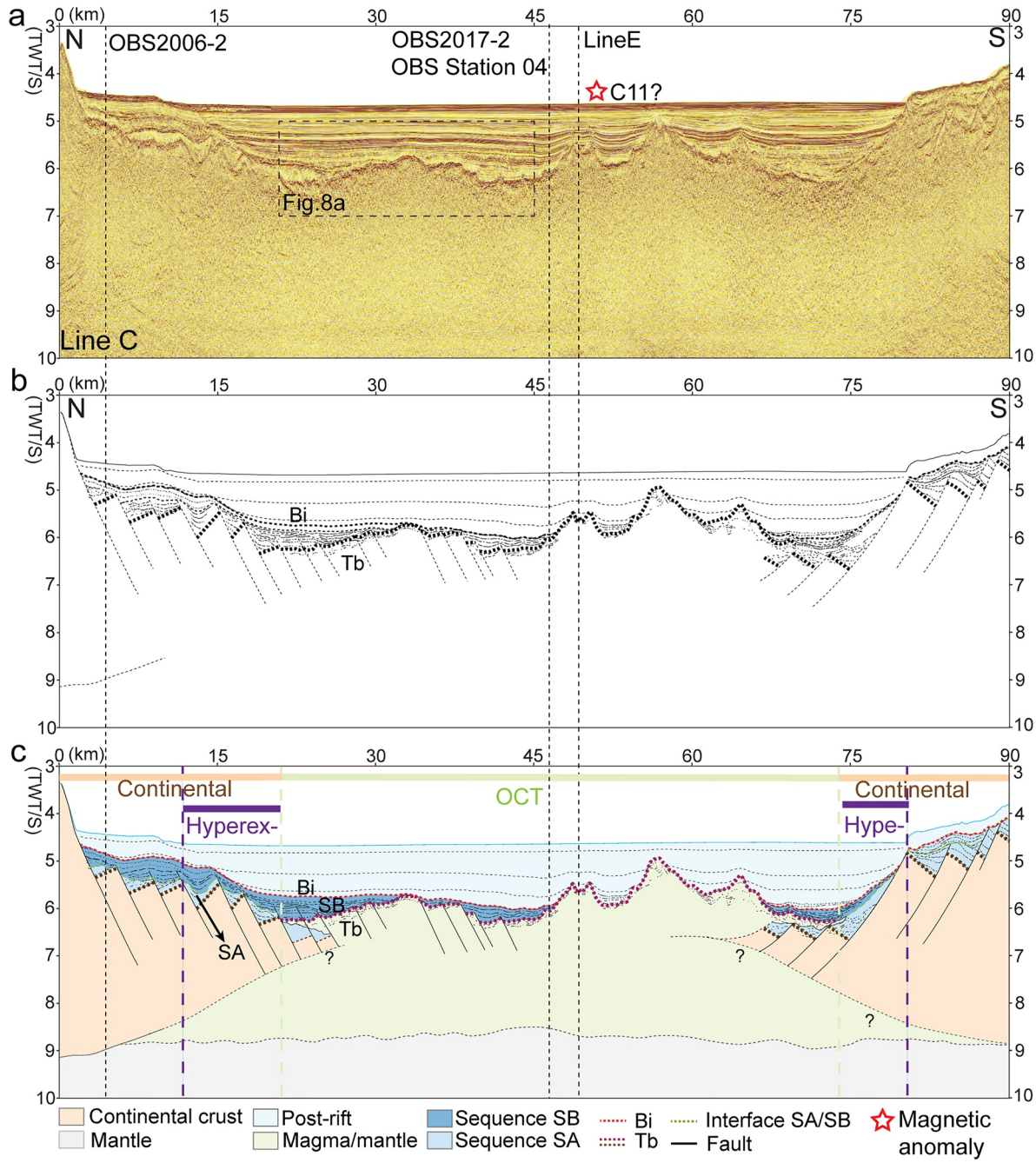

Figure 4. Seismic reflection section Line C across the tip of the propagator, for location see Figure 1. (a) Line C seismic reflection section in time with locations of cross line (thin dashed lines). (b) Line drawing of Line C, the bold dashed lines are Tb and Bi. (c) Seismic interpretation of Line C with first-order interfaces, stratigraphic horizons, and tectonic structures. Three sedimentary sequences (SA, SB and post-rift) were defined (for explanation see discussion section). Abbreviations used in the figure: Bi, Breakup interface; Tb, Top acoustic Basement.

south, Tb is affected by minor high-angle faults but remains sub-horizontal at ca. 4 s TWT between km 80 and 100. Between km 60 and 75, a crustal wedge offset by north-dipping faults pinches out at km 65 and at 8s TWT, which represents the location with the thinnest crust. Moho reflections are difficult to define but may correspond to a set of reflectivity that occurs at ca. 9 s TWT.

Based on our definition (see Section 3.3) we interpret the whole line as belonging to the continental domain. This is based on the observation of a Tb offset by high-angle faults and crustal thicknesses that are between 6 and 4 s

10.1029/2021TC007127

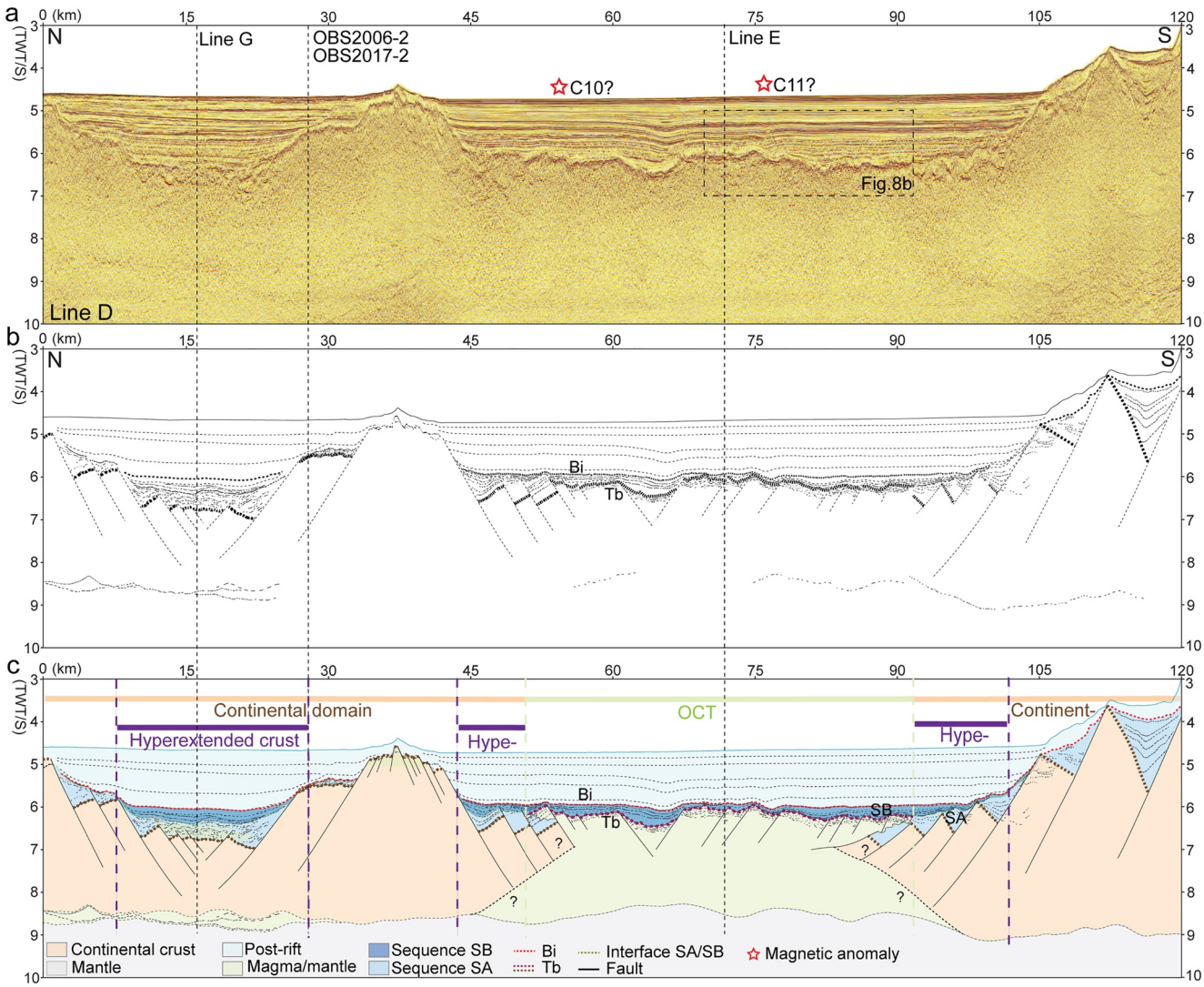

Figure 5. Seismic reflection section Line D across the tip of the propagator, for location see Figure 1. (a) Line D seismic reflection section in time with locations of cross lined (thin dashed lines). (b) Line drawing of Line D, the bold dashed lines are Tb and Bi. (c) Seismic interpretation of Line D with first-order interfaces, stratigraphic horizons, and tectonic structures. Three sedimentary sequences (SA, SB and post-rift) were defined (for explanation see discussion section). Abbreviations used in the figure: Bi, Breakup interface; Tb, Top acoustic Basement. Line D is the same line as seismic section L1, which has been published in Gao et al. (2016).

TWT in the north and south. The crust is strongly structured and tilted between km 30 and 55 and shows wedging shapes between km 65 and 80. The unequivocal magmatic crust is not observed in this section. We identify hyperextended crust between km 25 and 80.

4.1.2. Line B

Line B (Figure 3a) is parallel to Line A and ca. 18 km further east (for location see Figure 1). The seafloor is sub-horizontal between km 10 and 75 and at 4.5 s TWT (Figure 3b). Further south and north it is structured and rises up. Tb is offset and steps down across south-dipping faults from km 0 to 25. From km 25 to 40, Tb is offset by south-dipping faults, but the overall trend of Tb remains sub-horizontal. At km 45, a change from south- to north-dipping faults occurs and crustal wedging occurs from km 45 (tip of the wedge with a Tb i.e., at 8 s TWT) to a crust that is 3–4 s TWT-thick at km 70. Although at a crustal scale the northern margin shows a wedging/thinning of the crust, there is no tip to this wedge.

Relying on our definitions (see Section 3.3), we define the whole section as belonging to the continental domain. This is based on the topology of Tb which is offset across the whole line by high-angle faults. The overall shape

10.1029/2021TC007127

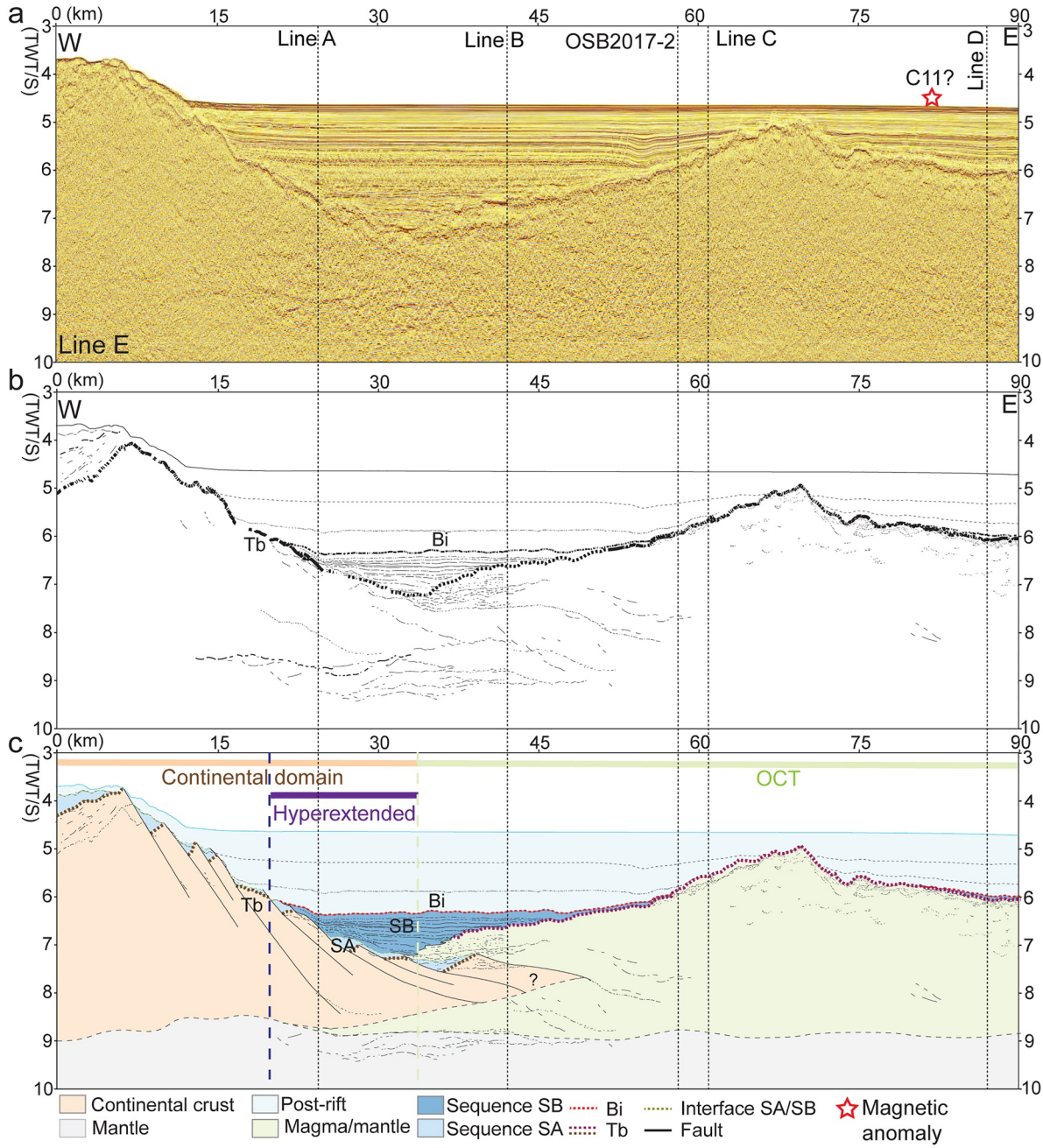

Figure 6. Seismic reflection section Line E, a strike line that is perpendicular to lines A to D (for location see Figure 1). (a) Line E seismic reflection section in time with locations of cross lines and magnetic anomalies C11 (thin dashed lines). (b) Line drawing of Line E, the bold dashed lines are Tb and Bi. (c) Seismic interpretation of Line E with first-order interfaces, stratigraphic horizons and tectonic structures. Three sedimentary sequences (SA, SB and post-rift) were defined (for explanation see discussion section). Abbreviations used in the figure: Bi, Breakup interface; Tb, Top acoustic Basement.

of the crust is wedging toward km 45, although a more complex crustal block with a relatively constant crustal thickness and made of tilted bocks can be observed between km 25 and 40. We consider this block to belong to the continental domain. We identify hyperextended crust between km 10 and 70. Possible magmatic additions are only observed at the center of the basin between km 45 and 55 (for description see below). Moho is essentially not observed due to the imaging depth that is limited to 8 s TWT for this line.

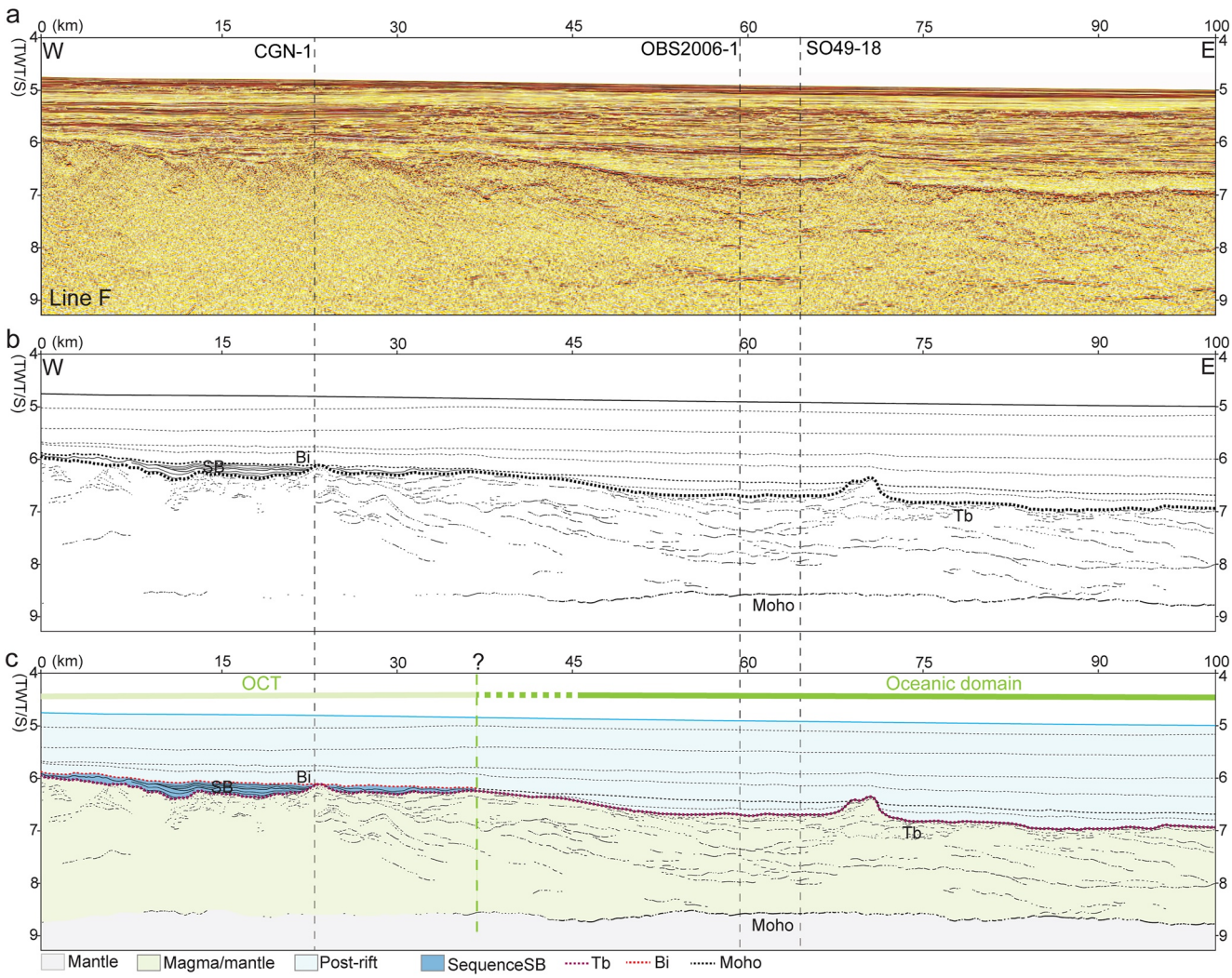

Figure 7. Seismic reflection section Line F, a strike line parallel to line E, located 21 km further north (for location see Figure 1). (a) Line F seismic reflection section in time with locations of cross lines. (b) Line drawing of Line F, the bold dashed lines are Tb and Bi. (c) Seismic interpretation of Line F with first-order interfaces, stratigraphic horizons and tectonic structures. Two sedimentary sequences (SB and post-rift) were defined (for explanation see discussion section). Abbreviations used in the figure: Bi, Breakup interface; Tb, Top acoustic Basement.

4.1.3. Line C

Line C (Figure 4a) is parallel to Line B and ca. 18 km further east (for location see Figure 1). The seafloor is sub-horizontal between km 3 and 80 and at 4.5 s TWT (Figure 4b). Further south and north, it is structured and rises up. Tb is offset and steps down across south-dipping faults in the north from km 0 to 20, and in the south from km 75 to 90 across north-dipping faults. Between km 20 and 75, Tb is defined by a strong reflection and is affected by normal faults with minor offset. Between km 20 and 35 Tb is tilted northward and from km 35 to 40 it steps down across south-dipping normal faults. Further south, Tb is made of 3 highs at km 50, 55, and 65 that we interpret as late volcanoes. To the south, Tb rises from 6.5 to 5.5 s TWT between km 55 and 75, across northward-dipping normal faults. Moho's reflections are difficult to identify in this section.

Relying on our definition (see Section 3.3), we define the continental domains between km 0 and 20 and km 75 and 90. This is based on the wedging shape of the crust and the oceanward stepping Tb offset by normal faults. We identify hyperextended crust between km 10 and 20 and between km 75 and 80. We define an OCT domain separating the two continental domains between km 20 and 75. The limit is set where a break in the slope and a change in the dip of Tb occur. This change is accompanied by a change in the topology of Tb, from fault-structured, bookshelf like in the continent, to rougher but still fault-structured in the OCT (Figure 8). Fault offsets

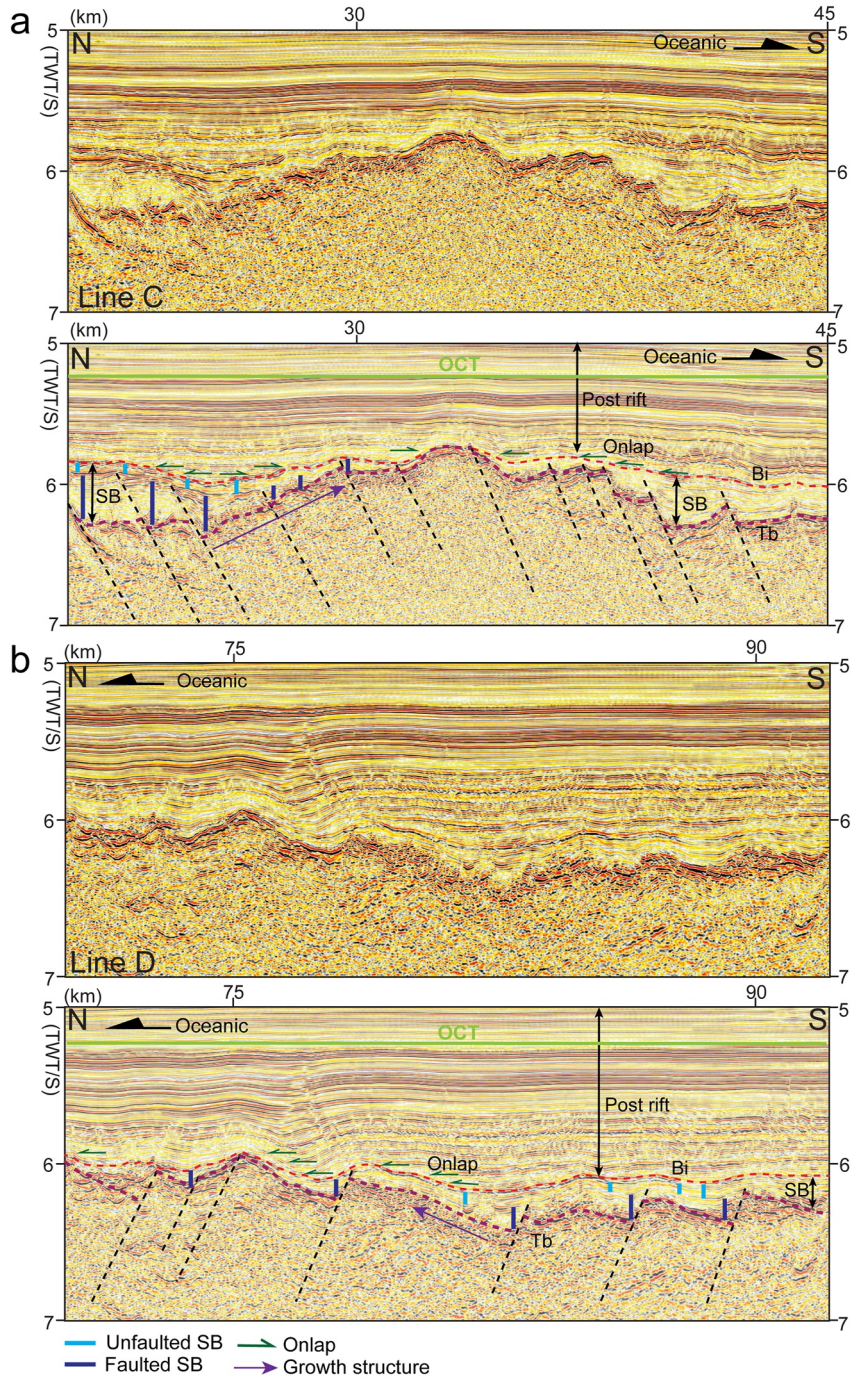

Figure 8. Close ups of seismic reflection sections showing top basement and the relation between normal faults and the sedimentary sequence SB in the Ocean Continent Transition. Note that the lower part of the sedimentary sequence SB is fault-bounded (dark blue columns); in contrast, the upper part is sealing the faults but is locally tilted, suggesting a syn-tectonic deposition. The red line corresponds to the breakup interface (Bi) and separates SB from reflections that are horizontal and show passive infill. (a) Close up on Line C (for location see Figures 1 and 4a). (b) Close up on Line D (for location see Figures 1 and 5a).

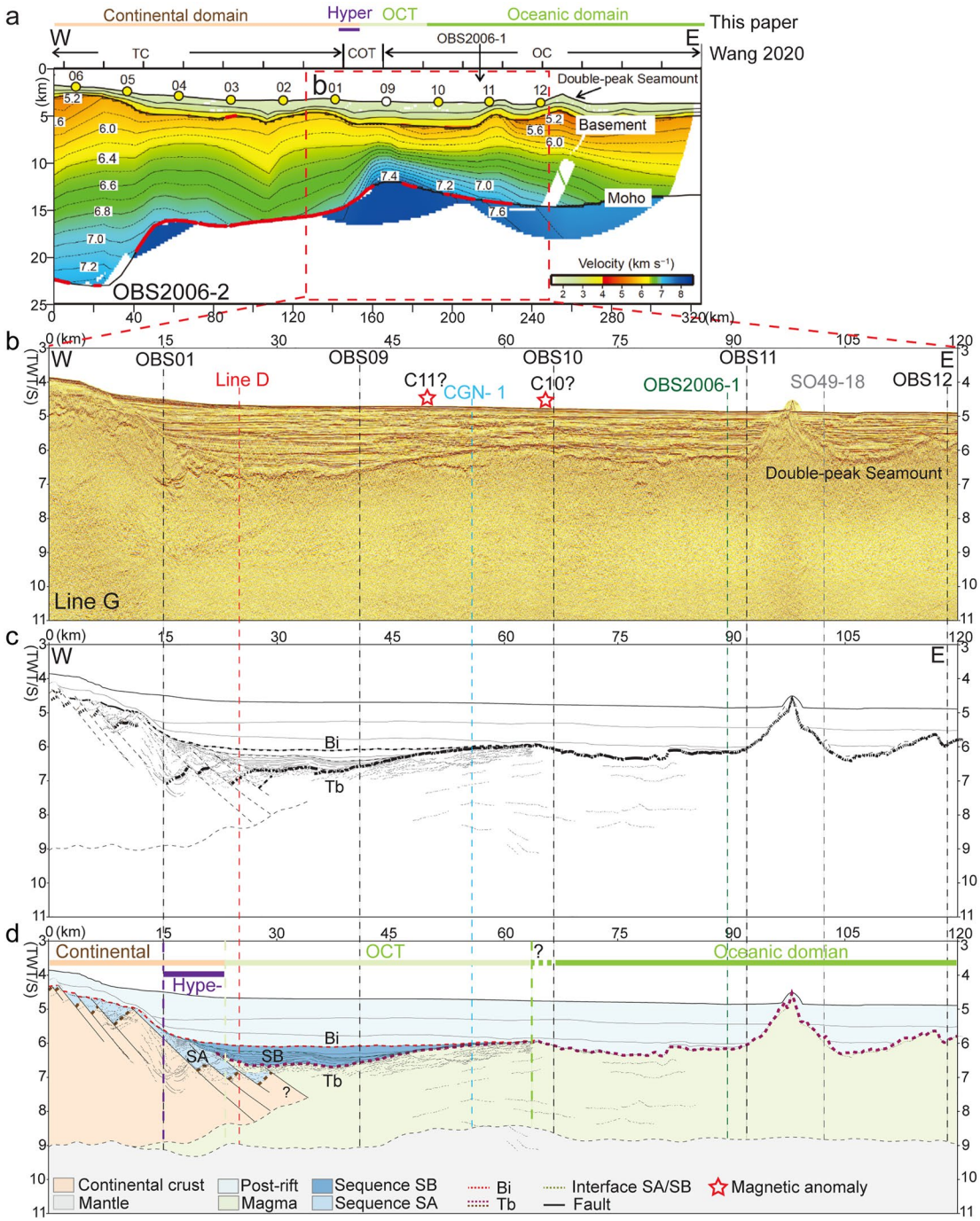

Figure 9. Seismic refraction section OBS2006-2 and seismic reflection section Line G, strike lines parallel to lines E and F. Line G and OBS2006-2 are 9 km apart (for location see Figure 1). (a) OBS2006-2 velocity structure of the inverted model obtained using Tomo2D software, for more details see Wang et al. (2020). The red dotted box shows the projected location of Line G. (b) Line G seismic reflection section in time with location of cross lines and OBS station points (thin dashed lines). (c) Line drawing of Line G, the bold dashed lines are Tb and Bi. (d) Seismic interpretation of Line G with first-order interfaces, stratigraphic horizons, and tectonic structures. Three sedimentary sequences (SA, SB and post-rift) were defined (for explanation see discussion section). Abbreviations used: OCT=COT, Ocean-Continent Transition; TC, Thinned Continental crust; OC, Oceanic crust.

are, however, much smaller, and magmatic additions can be recognized. No unequivocal oceanic crust can be observed in this section.

4.1.4. Line D

Line D (Figure 5a) is parallel to Line C and ca. 27 km further east (for location see Figure 1). The seafloor is sub-horizontal between km 0 and 105 and lies at 4.5 s TWT (Figure 5b). Further south it is structured and rises up. Tb is more complex to the north, displaying a graben-type structure bounded by north- and south-dipping faults between km 0 and 35. This structure is limited southward by a basement high that lies between km 30 and 45. From km 45 to the south, Tb is offset by south-dipping faults and remains sub-horizontal between km 50 and 90. There, Tb is defined by a strong reflector offset by normal faults with minor displacement. South of km 90, Tb is offset first by minor northward-dipping faults with small offsets, then major northward-dipping faults with large offsets. Moho reflections are difficult to define but may correspond to a set of reflectivity that occurs at ca. 9 s TWT.

Relying on our definition (see Section 3.3), we define the continental domain between km 0 and 50 and south of km 90. This interpretation is based on the wedging of the crust in the north and the south and the structured Tb offset by oceanward-dipping normal faults. We define the block between km 30 and 45 as belonging to the continental domain, although Tb may coincide with minor magmatic additions. Beneath the graben and south of the block, we identify wedging and fault-structured hyperextended crust between km 10 and 30, between km 45 and 50, and between km 90 and 100. We interpret the domain from km 50 to 90 as an OCT with a crust primarily made of igneous material. The crust displays an irregular Tb, but not a wedging shape.

4.1.5. Line E

Line E (Figure 6a) is a strike line perpendicular to lines A to D (for location see Figure 1). The seafloor is sub-horizontal and lies at ca. 5 s TWT with the exception of km 0 to 15, where Tb rises up to less than 4 s TWT (Figure 6b). Tb is well imaged and can be observed across the whole line. From km 5 to 30, Tb dips toward the east from 4 to 7.5 s TWT. From km 30 to 70, Tb rises to 5 s and then drops down to 7 s TWT over a structure that is quite symmetric. At the intersection with line C, the seismic nature of the crust corresponds to magmatic additions with a general thickening of the crust to the east (see an intersection with line C in Figure 4b), suggesting the existence of a magmatic ridge. Moho reflections are difficult to define but may correspond to a set of reflectivity that occurs at ca. 9 s TWT between km 15 and 50.

Relying on our definition (see Section 3.3), we define the continental domain to occur between km 0 and 35 and we interpret the rest of the section to belong to the OCT domain made of first hybrid- and then fully magmatic crust. The interpretation of the continental domain is based on the wedging shape of the crust with a Tb offset by normal faults. Its eastern termination corresponds to hyperextended crust between km 20 and 35. In the remaining part of the section, Tb is smooth to slightly uneven and dips continent-ward.

4.1.6. Line F

Line F (Figure 7a) is a strike line parallel to line E, located ca. 21 km further north. This line images the eastward continuation of the center of the V-shaped basin (for location see Figure 1). The seafloor is sub-horizontal and lies at ca. 5 s TWT. Tb is well imaged and can be observed across the whole line as a complex and uneven surface from km 0 to about 45 and as a strong reflection from km 45 to 100, except for a volcano-shaped body at km 70. Moho reflections are well imaged and at 9 s TWT from km 55 to 100, while further west the Moho cannot be observed.

Based on the box-shaped architecture of the crust, the smooth Tb and the passive infill of the overlying sediments, we define the oceanic domain as lying between km 55 and 100. We define the domain between km 0 and 55 as belonging to the OCT domain since it does neither show a wedging of the crust, nor a structured Tb offset by normal faults. It is worth noting that there is a change in the intra-basement reflectivity in the OCT from relatively transparent in the west to more reflective and displaying seaward dipping reflectors in the east. Reflectivity in the oceanic domain is sub-horizontal and layered.

4.1.7. Line G

Line G (9a) is a strike line parallel to lines E and F and just north of the OBS2006_2 line that is shown, for comparison, in the same section (for location see Figure 1). Seafloor is sub-horizontal and lies at ca. 5 s TWT

except for its western termination (9b). Tb is well imaged from km 20 to 120 and more difficult to define westwards of km 20. We interpret Tb to be offset by faults and to step down from ca. 4 s TWT to ca. 7 s TWT, indicating a wedging of the crust that tips out at ca. km 35. Tb is defined as a strong reflection from km 20 to the end of the section in the east. From ca. km 20 to 60 it dips toward the west, that is, toward the continent. Faint and discontinuous Moho reflections can be seen west of km 60 at ca. 9 s TWT while Moho reflections are difficult to observe further east.

Based on our definition (see Section 3.3), we define the wedge-shaped crust with a fault-structured Tb west of km 20 as belonging to the continental domain. We identify hyperextended crust between km 15 and 25. We define an OCT domain between km 20 and 65, which displays a continent-ward dipping Tb that terminates eastward at a basement high at km 65. The crust east of this high shows a horizontal, smooth Tb (except for a volcano at km 95) and passive infill qualifying as an unequivocal oceanic domain.

4.1.8. Crustal Structure and Domains: Main Observations

The interpretation of seismic reflection lines located at the tip of the NW-SCS enables us to characterize the main interfaces, domains, and domain boundaries. In the continental domain, Tb is offset by faults and tilted, and lies between 3 and 7s TWT. Moho lies globally at 9 s TWT. In the OCT domain, Tb displays a rough morphology and ranges between depths of 6 and 7.5 s TWT and Moho lies between 8 and 9 s TWT. In the oceanic domain, Tb and Moho are parallel and the crust is 2 s TWT-thick. Tb is smooth and lies at 6.8 s TWT while Moho lies at 8.8 s TWT.

4.2. Sedimentary Sequences

Compactable sediments along lines A to G are shown in Figures 2–9 are contained between Tb and the seafloor. They can be subdivided into a syn-rift and a post-rift mega-sequence. The occurrence of pre-rift sediments over continental crust is likely, but their presence is difficult to confirm without drill hole data. We, therefore, include them in the acoustic basement capped by Tb. Distinguishing between the syn- and post-rift sequences is difficult in a polyphase rift system where strain is supposed to localize with time and where the syn-tectonic sequence is diachronous across both dip and strike sections (Chenin et al., 2021; Luo et al., 2021). Indeed, since sediments deposited during the time of rifting can be deposited outside the tectonically active zone, the syn-rift sequence can include both syn- and post-tectonic sediments, and the latter are difficult to distinguish from post-rift sediments. In this study, we subdivide the syn-rift mega-sequence observed over the continental and OCT domains into two sequences, referred to as SA and SB, respectively. SA and SB are correlated across seismic sections based on both their seismic facies. The geometric control resulting from the numerous intersections between the studied seismic sections allows us a relatively reliable mapping (cf. Figure 1 and the trace of crosscutting seismic sections displayed in Figures 2–9). SA does not occur over the OCT. SB encompasses the first sediments deposited over the OCT (Figure 8). The post-rift mega-sequence is the first sedimentary sequence deposited over the oceanic domain showing passive infill (Figure 8). A characteristic of the post-rift mega-sequence is that it does not show syn-tectonic architectures in the study area. The limit between the syn- and post-rift mega-sequences is defined as the breakup interface Bi, which can be mapped across the study area as explained below.

The first sequence (SA) is best defined along Line B (Figure 3c). It shows growth structures bounded by normal faults offsetting Tb in the continental domain. SA is floored by either Tb or faults, and its sediments thicken into faults. The top of SA is largely continuous and it locally seals faults, suggesting relatively high sedimentation rates. In dip lines C and D and in strike line E (Figures 4c, 5c and 6c), regular and relatively continuous reflections characteristic of sedimentary deposits interfinger with strong and discontinuous reflections associated with cluttered and more massive reflectivity that may represent magmatic additions. Thus, SA either interferers or is intruded by what we interpret as magmatic additions, but we can never see SA downlapping or onlapping onto magmatic Tb in the OCT. The use of dip and strike lines allows us to identify and correlate SA across the whole tip of the NW-SCS. It systematically occurs over faulted and wedging crust.

The second sequence (SB) is best defined along line C (Fig. 4c) and a close up is shown in Figure 8a. SB onlaps continent-ward either onto SA or directly onto the basement, and down- or onlaps outboard onto a reflective Tb, interpreted as the top of a magmatic crust belonging to the OCT. SB wedges out oceanward over the OCT (lines C, D, E, G; Figures 4c, 5c and 6c, and 9c), and shows growth structures linked to minor normal faults that offset Tb in the OCT (Figure 8a). Similar observations can be made along the dip line D (Figures 5c; 8b) or on the strike

lines E and G (Figures 6c and 9c). Along line E, SB is tilted continent-ward and is onlapped by younger post-rift sediments (Figure 6c). On lines A and B (Figures 2c and 3c), SB occurs over SA and does only show minor thickness changes across faults. In these lines, SB is clearly post-tectonic and shows passive infill geometries. The mapping of SB in the western tip is based on correlations along the strike of line E (Figure 1). Oceanward, as shown along lines F and G (Figures 7c and 9c), SB wedges out and does not occur over oceanic crust.

The top of the SB sequence referred to as Bi, is best defined on lines C to G (Figures 4c, 8a, and 9c). Along line C, Bi coincides with the base of passive infill. Along line G, Bi terminates against the basement high that marks the end of the continent-ward tilting of the Tb in the OCT and forms the limit to the first oceanic crust. This geometrical relationship defines the relative age of Bi corresponding to the time of lithospheric breakup and formation of the first oceanic crust at the tip of the NW-SCS. Based on the correlation of Bi across the dip and strike lines shown in Figure 1, we can trace Bi across the tip of the NW-SCS. Oceanward, Bi either onlaps on the outer high located at the oceanward limit of the OCT (line G; 9c), or downlaps onto the first oceanic crust (line F; Figure 7c). Continent-ward, Bi lies within the post-tectonic sequence (line A; Figure 2c). Thus, rift cessation at the tip of the NW-SCS in the west predated the onset of seafloor spreading further east.

The third sequence defined in our study is the post-rift mega-sequence. It overlies Bi, does not show any growth structures throughout the study area and it is the first sequence overlying mature oceanic crust. In the following, we will not further discuss the post-rift mega-sequence since the aim of this study is to discuss the tectono-stratigraphic history/signature of breakup at the tip of the NW-SCS.

5. Mapping Rift Domains at the Tip of the NW-SCS

5.1. Mapping Rift Domains Based on Seismic Reflection Data

In the previous section, we defined rift domains based on seismic reflection interpretations from the tip of the NW-SCS. The aim of this section is to transform these results into a rift domain map. We use the methodology of Tugend et al. (2014) to create a rift domain map. Definitions of rift domains and domain boundaries are provided in Section 3.3. A rift domain map neither shows structural details nor does it consider the composition of the underlying crust, although the link between lithologies and rift domains is apparent for the oceanic and continental domains.

To construct the map shown in Figure 10b, we used all lines presented in this manuscript, additional proprietary lines, as well as lines that are already published (for line locations see Figures 10a and 10b). We applied the interpretation approach described above to all the lines of the survey that are shown in Figure 10a. This allowed us to produce a rift domain map that is well constrained, in particular at the tip of the V-shaped NW-SCS. Indeed, for each of the seismic lines shown in Figure 10a and crossing the study area, we defined the rift domain boundaries and linked them into a continuous domain boundary. In the continental domain, we also used the refraction data (for description see next section). A comparison of the crustal thickness map produced by Gozzard et al. (2018) (Figure 10a) with the rift domain map (Figure 10b) shows that there is a first-order correspondence between crustal thickness defined by gravity inversion (Figure 10a) and the domain boundaries defined from seismic reflection data (Figure 10b). This result is not surprising since crustal thickness and thinning gradients (i.e., wedge-vs. box-shape; see Luo et al. [2021]) are first-order characteristics of rift domains. However, since the two maps are independent of each other, the good fit supports the validity of our approach. The main observation is that the continent-ward limit of the hyperextended domain coincides with a change in the thinning gradient (Figure 10a), while the boundaries between hyperextended and OCT domains, and between OCT and oceanic domains, are difficult to identify in a crustal thickness map. These domain boundaries involve different types of crust with different velocity structures and can therefore be imaged using seismic refraction data. However, as discussed later, they are better and more precisely defined using high-quality, long offset seismic reflection data.

Our rift domain map (Figure 10b) shows a complex crustal structure at the tip of the NW-SCS that includes three crustal blocks, namely continental China to the north, the Macclesfield Block to the south, and the Paracel Block to the west. These domains of thicker continental crust are separated by hyperextended domains in the west. Eastward, an oceanic domain appears, and the related crustal structure is simpler. From the map, it is obvious that the tip is not a simple structure. The distribution of hyperextended domains is complex and does not show the commonly assumed idea of a wide and distributed rift in front of a propagating oceanic domain. It is surprising that the tip of the oceanic domain does not follow the trend of the hyperextended domains in its frontal part.

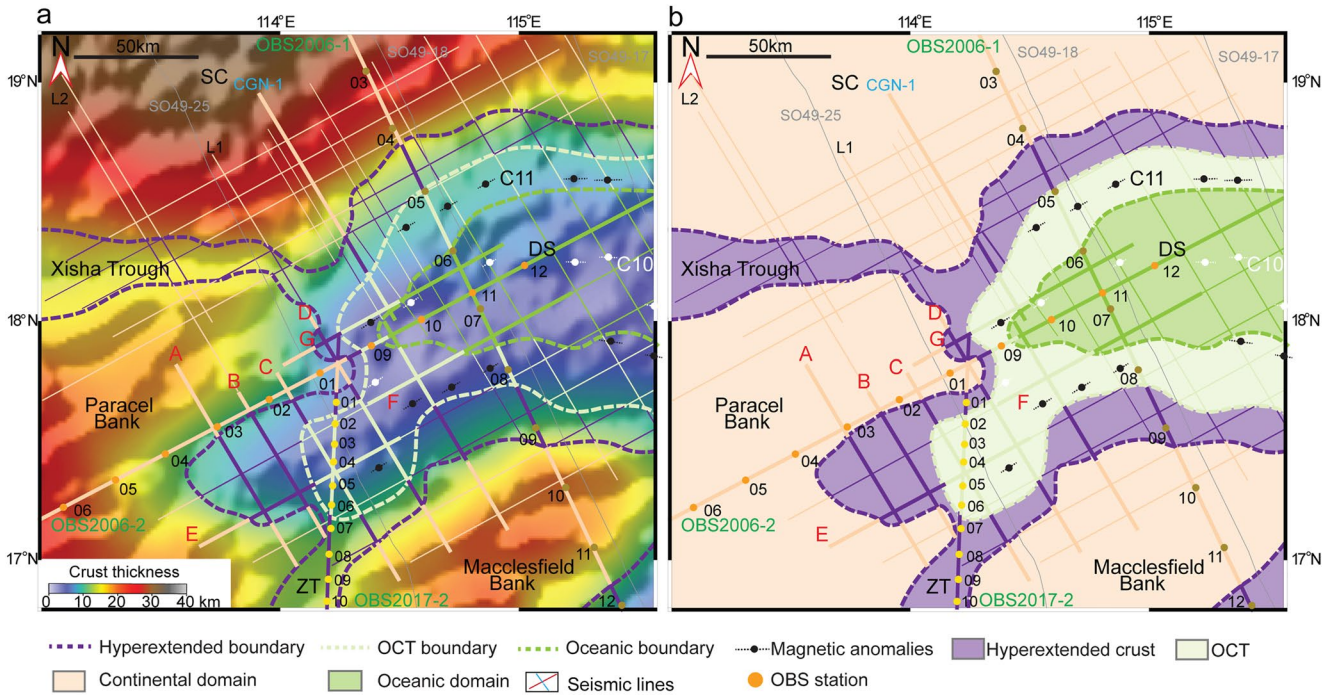

Figure 10. (a) Crustal thickness map from Gozzard et al. (2018) with all used seismic lines (for labels see Figure 1) and rift domains. (b) Map showing rift domains in the study area in the NW-SCS. The domain boundaries are derived from seismic interpretations, by tracing the limits of the hyperextended, OCT, and oceanic domains.

This is even more surprising considering that in the east, the oceanic domain splits the hyperextended and OCT domains evenly on both sides.

5.2. Nature of Crust at the Tip of the NW-SCS: Constraints From Seismic Refraction Data

In the absence of drill hole data, it is impossible to determine unambiguously the lithologies forming the crust. In distal, sediment-rich margins it is always difficult to penetrate the basement, and where it has been done, it was limited to basement highs (e.g., IODP Legs 367, 368 and 368X SCS; Larson et al. [2018]; ODP Legs 103, 149, 173 and 210 Iberia-Newfoundland; Tucholke et al. [2007]). Seismic refraction and potential field data can provide indirect constraints on the composition of the crust, however, such methods are non-unique, since velocities, densities and magnetic properties cannot be assigned to one lithology only. Péron-Pinvidic et al. (2016) showed that significant mismatches may arise between structural interpretations based on seismic reflection and refraction data and/or on potential field methods for distal rifted margins. Here we discuss the results of three seismic refraction lines crossing the tip of the NW-SCS (Figure 11; for the location of lines see Figure 1). Lines OBS2006-1 and OBS2006-2 have been published and described by Wu et al. (2012), and line OBS2017-2 by Y. Li et al. (2021). Here we present these sections to compare both our seismic reflection interpretation (9) and our rift domain map (Figure 10) with the seismic refraction data.

Refraction line OBS2006-2 and reflection line G are shown in Figures 9a and 9b are parallel lines only 9 km apart (for location see Figure 1). Thus, comparing the two lines offers the possibility to link a velocity structure (OBS data) with a rift domain interpretation. As shown in 9, OBS01 samples the velocity structure of the hyperextended crust, OBS09 that of the OCT, and OBS11 that of the oceanic domain. From the velocity structure shown in 9a, it is clear that the three domains are characterized by different velocity structures, indicating different crustal compositions. The first main observation is that crustal thinning from ca. 10 km at OBS 01 to ca. 6 km at OBS 09 occurs in the hyperextended domain and is linked to a narrow rise of the Moho. A change in the crustal velocity structure across the hyperextended and OCT domains as shown by OBS01, OBS09, and OBS10 is compatible with the interpreted change from a hybrid to a fully magmatic crust in the OCT shown in Figure 9d. The thickening of the crust oceanward in the OCT shown by OBS09 and OBS10 is consistent with the observed uplift and continent-ward tilting of Tb. Unfortunately, the oceanward part of the section is perturbed by the emplacement

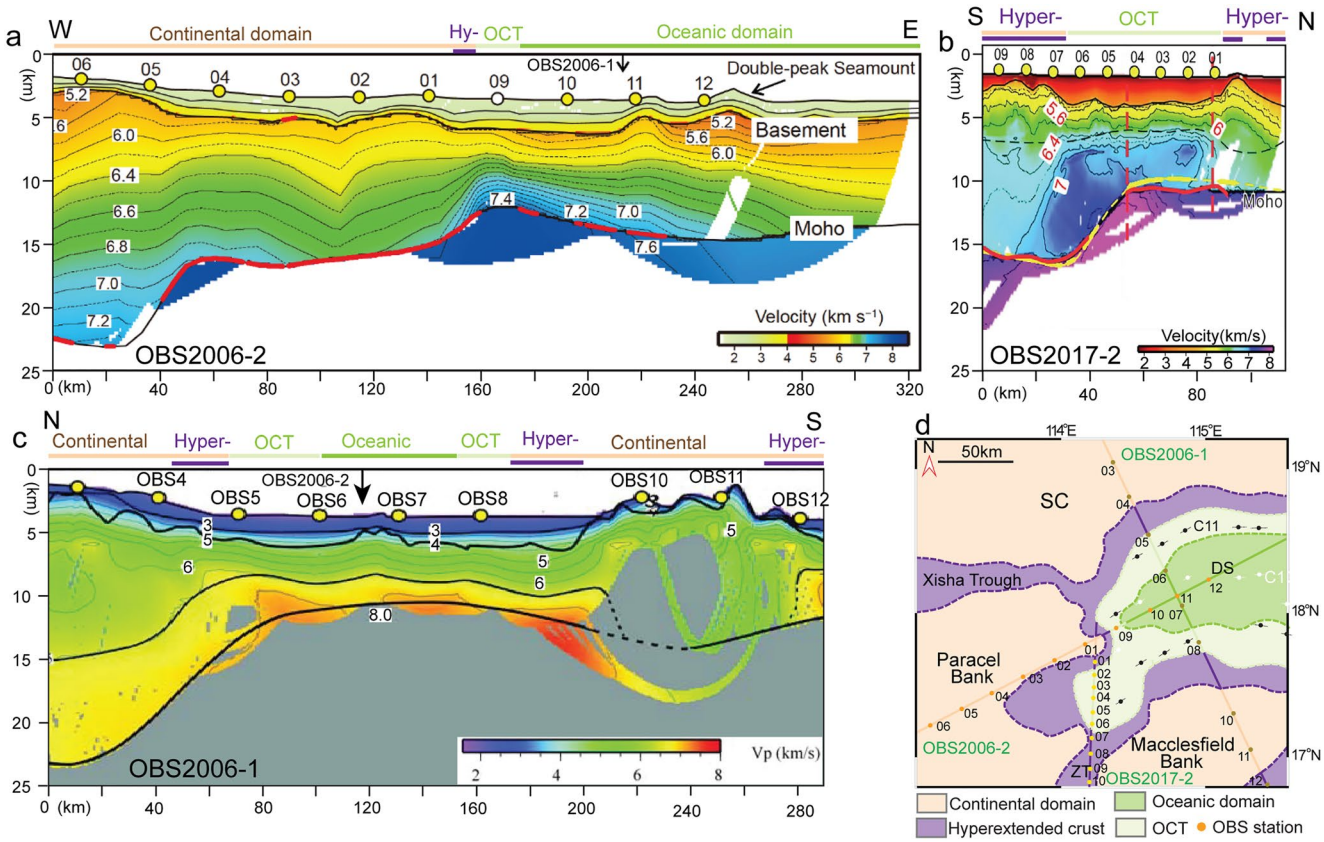

Figure 11. (a) Velocity model for seismic refraction line OBS2006-2 from Wang et al. (2020) crossing the tip of the NW-South China Sea (NW-SCS). (b) Velocity model for seismic refraction line OBS2017-2 from Li et al. (2021) crossing the tip of the NW-SCS. (c) Velocity model for seismic refraction line OBS2006-1 from Wu et al. (2012) and Ding et al. (2012) imaging a section through the conjugate margins in the rear of the NW-SCS. (d) Rift domain map with locations of refraction lines.

of late volcanoes, well imaged in the seismic reflection section at km 95 and showing that late magmatic activity may have resulted in local thickening of the oceanic crust.

In Figure 11d, we plot the position of the three seismic refraction velocity models (Figures 11a–11c) on the rift-domain map and show, along each refraction model, the imaged domain (bar with the color of the domain above the line). This allows us to determine the range of velocities and thicknesses for each mapped domain. The crustal thickness does not significantly change across the distal margin: the hyperextended domain ranges from 10 to 6 km showing a wedging oceanwards; the OCT is thinnest on its continent-ward side (ca. 6 km) and slightly thickens oceanward to 7 or 8 km; the thickness of the oceanic crust is difficult to determine due to the existence of late magmatic additions on OBS2006-2 but is on the order of 5–6 km along OBS2006-1. In contrast to the crustal thickness variations that may not allow differentiation of these domains, the velocity structure shows important differences between the continental and oceanic domains. The velocity structure of the OCT shows a characteristic, gradual change in velocity and crustal thickness across the OCT. The main difference between the continental and oceanic crusts is the high-velocity layer characterizing the lower crust in the oceanic domain. For all models, the limit between the hyperextended domain and the OCT coincides with an abrupt rise of the Moho and a significant thinning of the crust over a narrow region. In contrast, the transition to oceanic crust seems more gradual both in terms of seismic velocity and crustal shape.

5.3. Comparison With Existing COB Maps and Potential Field Data

In Figure 12a, we compare our rift domain map with previously published locations of the Continent-Ocean Boundary (COB), spreading centers, and other structures. Zhang et al. (2012) (light blue lines in Figure 12) defined the COB and abandoned spreading center using magnetic data. This interpretation is similar to that of C. Li et al. (2012) (line in Figure 12). Their COB includes parts of our hyperextended crust and OCT. It is also

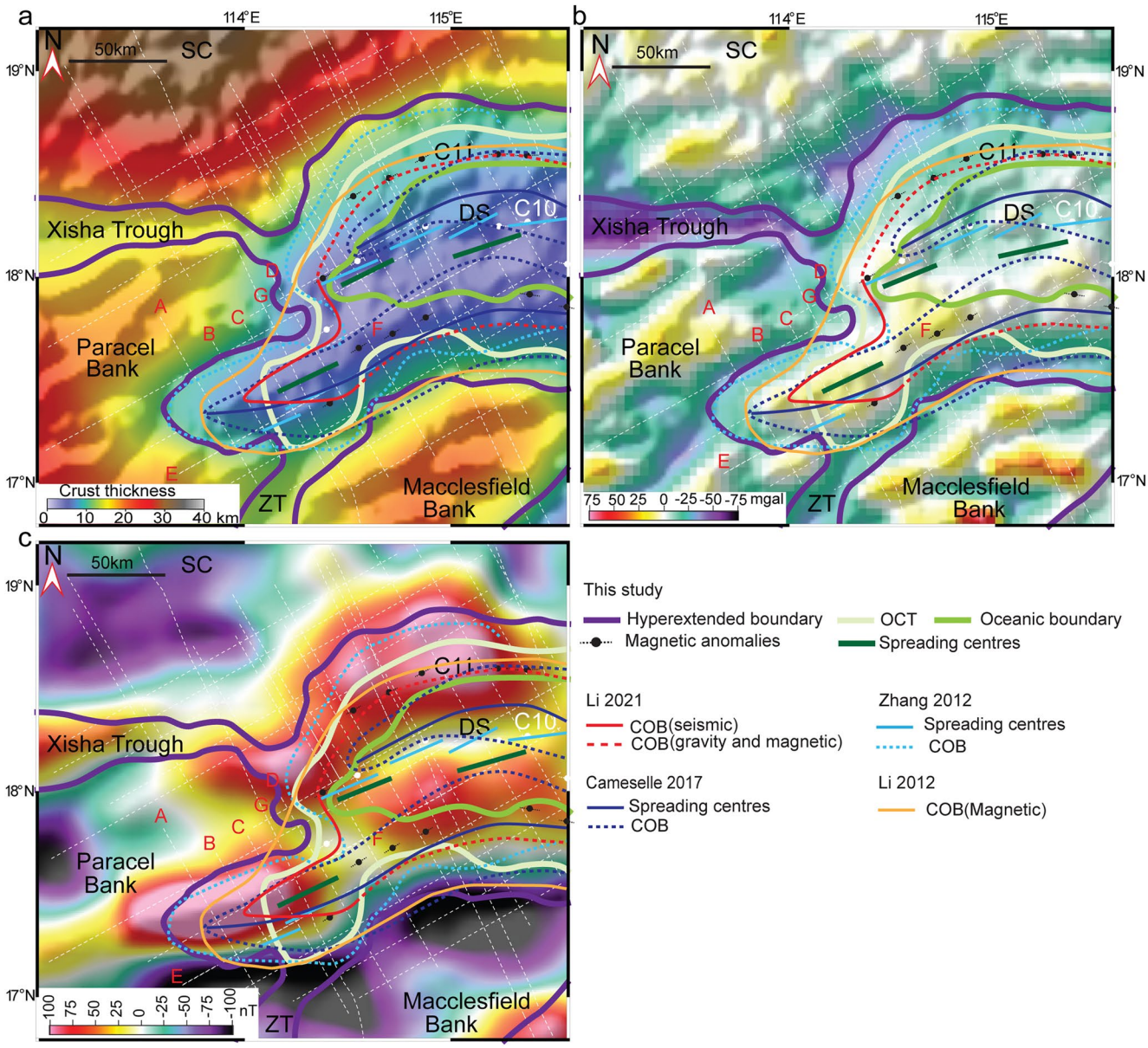

Figure 12. Comparison of our rift domain map with previously published locations of the continent oceanic boundary (COB), spreading centers and other structures at the tip of the NW-South China Sea. (a) Crustal thickness map from Gozzard et al. (2018). (b) Free-air gravity anomaly map. (c) Magnetic anomaly map. Maps from Gozzard et al. (2018). The light blue solid line and the light blue dashed line show the location of the spreading center and the location of the COB interpreted by Zhang et al. (2012), respectively. The solid red line marks the location of the COB constrained by seismic results, while the dashed line represents the COB deduced from gravity and magnetic data by Li et al. (2021). The dark blue solid line and dashed line show the location of the spreading center and COB interpreted by Cameselle et al. (2017) based on multichannel seismic data. The orange solid line represents the COB deduced from magnetic data by Li et al. (2012).

interesting to see that these authors proposed a transform fault separating two oceanic segments. Cameselle et al. (2017) (dark blue lines in Figure 12) used seismic reflection data and gravity data to define two spreading centers with very narrow COBs. They interpreted the southern ridge as the older one and the northern as the younger one and suggested a ridge jump. These authors mapped most of what we consider oceanic and OCT domains as the thinned continental crust. More recently Y. Li et al. (2021) (red lines in Figure 12) defined the COB in the NW-SCS based on seismic reflection and refraction data in the western part of the tip and using gravity and magnetic data for the eastern parts. Their interpreted COB lies within our OCT.

The differences between the interpretations show that: (a) defining the location of the breakup is complex and non-unique and depends on the used dataset, method, and definition of the COB; (b) the different interpretations

still show similarities with our mapped boundaries, for instance, the COB of Zhang et al. (2012) matches with the continent-ward part of our hyperextended domain; the COB of Li et al. (2021) corresponds to the continent-ward limit of our OCT; and the location of the northern spreading ridge and segmentation of Zhang et al. (2012) match with the location of our oceanic domain. In these cases, the methods and/or observations may provide similar results, but the definitions of domains/crusts are different. However, some interpretations are difficult to reconcile, like for instance the COB of Cameselle et al. (2017) that conflicts with most other interpretations.

A comparison between the rift domains mapped in the different studies presented above and free air gravity data from Gozzard et al. (2018) is shown in Figure 12b. A good correlation exists between the hyperextended domain and a negative gravity anomaly, which is compatible with the existence of a strong crustal thinning. The anomaly is sharper and stronger on the continent-ward side than on its oceanward side, which is compatible with the crustal thickness variations observed from seismic data across the margins in the NW-SCS.

A comparison between the rift domains mapped from the different studies and magnetic data is shown in Figure 12c. Within the magnetic map, low values correlate well with thick continental blocks. An exception is a hyperextended domain imaged by line OBS2017-2 separating the Macclesfield from the Paracel banks. Within the more extended/oceanic domains, three positive magnetic anomalies can be observed. One is overlying oceanic crust and parallel to oceanic magnetic anomalies. This anomaly correlates well with the oceanic domain that we mapped. A second, major anomaly can be recognized further north. It is parallel to the hyperextended and OCT domains and shows an abrupt termination toward the west. Although this anomaly is parallel to magnetic anomaly C11 as well as to the limits between the hyperextended domain and OCT, it remains unclear what may be the origin of this anomaly. The most surprising is that nothing comparable can be found on the conjugate margin. Even along the refraction line OBS2006-1 crossing the anomaly, nothing particular can be found below OBS5 which is located right above the anomaly. Similarly, the anomaly overlying the tip of the V-shaped basin occurs over hyperextended crust where we interpret tilted blocks (see line B; Figure 3a). Some evidence for magmatic additions can be seen and are shown along line B (Figure 3c) but it is difficult to determine if this can explain the magnetic anomaly. The strong magnetic anomaly may explain why most interpretations (Cameselle et al., 2017; C. Li et al., 2012; Y. Li et al., 2021; Zhang et al., 2012) put the tip of the oceanic propagator at this location, which is, however, inconsistent with seismic reflection observations.

5.4. Distribution of Sedimentary Sequences at the Tip of the NW-SCS

We defined and discussed SA and SB as well as Tb and Bi in Section 4.2. Maps showing the distribution of SA, SB and the post-rift sequence are shown in Figure 13. Since we were able to map these sequences along all lines (see Figure 10a) and not only along the lines presented here, we are confident that SA, like SB, is of the same age across the small extent of our study area, which is not necessarily true for the whole NW-SCS. We also assume that Bi represents a time marker in the study area and corresponds to the timing of lithospheric breakup in the eastern part of the study area. Regardless of whether we regard dip or strike lines, Bi and Tb converge basinward/oceanward and Bi onlaps or downlaps onto the location of lithospheric breakup (i.e., the outer limit of the OCT), as expected for an interface defined as a "breakup interface". The outer limit of the OCT defines the oceanward limit of the extent of SB. Away from this limit, toward the north, south, and west, the syn-rift mega-sequence bounded by Tb and Bi (i.e., SA plus SB) thickens, as observed along the sections shown in Figures 2c–9c. Moreover, we systematically observe that SA wedges out first, while SB continues further oceanward. However, in contrast to SB, the point/line where SA wedges out to zero is difficult to observe. For all sections where the OCT can be defined (lines C, D, E and G; Figures 4c, 5c and 6c, 9c), SA appears to either terminate into or to be overlain by magmatic additions. In all sections we consider SA to stop at the termination of continental crust (see Figure 14c), which is an interpretation. In our maps, we put the oceanward termination of SA at the limit between the continental and OCT domains, that is, at the first appearance of massive magmatic additions. However, we cannot exclude that SA continues underneath the magmatic additions (as shown in Figure 14c) that form the continent-ward edge of the OCT. In our interpretations, we show a sandwich-like position of SA between a continental Tb and the magmatic Tb, the latter overlaying the newly-created crust belonging to the OCT. When mapping Bi across lines from the continent toward the tip of the NW-SCS, we observe that this time marker post-dates active faulting in this segment but corresponds to lithospheric breakup in the neighboring eastern segment.

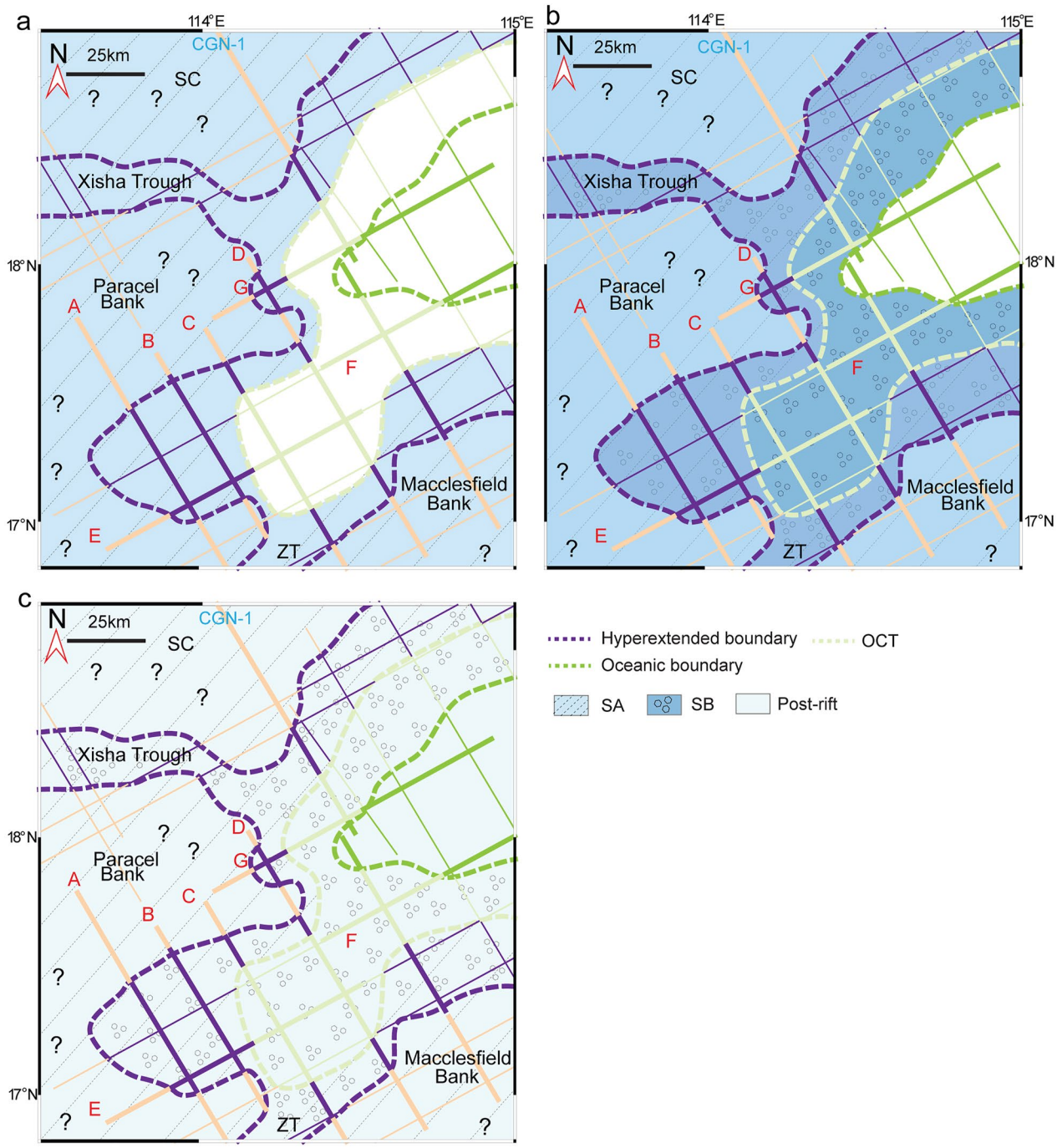

Figure 13. Maps showing the distribution of SA, SB, and the post-rift sequence at the tip of the NW-South China Sea. (a) Distribution of SA. (b) Distribution of SA and SB. (c) Distribution of SA, SB and the post-rift sequence. Abbreviations used in the figure: SC, South China Continental Margin; ZT, Zhongsha Trough.

6. Discussion

In this study, we described and mapped rift domains at the tip of the NW-SCS based on a high-resolution seismic reflection dataset. We produced a rift domain map and compared it with seismic refraction, magnetic and gravity field data, as well as previously mapped COBs. We also analyzed and defined syn-hyperextension and syn-breakup sedimentary sequences (SA and SB, respectively) and mapped them across the study area. This work allows us to now discuss the 3D architecture of the crust at the tip of the NW-SCS, its tectono-magmatic evolution related to breakup, and to examine how breakup evolved and finally ceased in the NW-SCS.

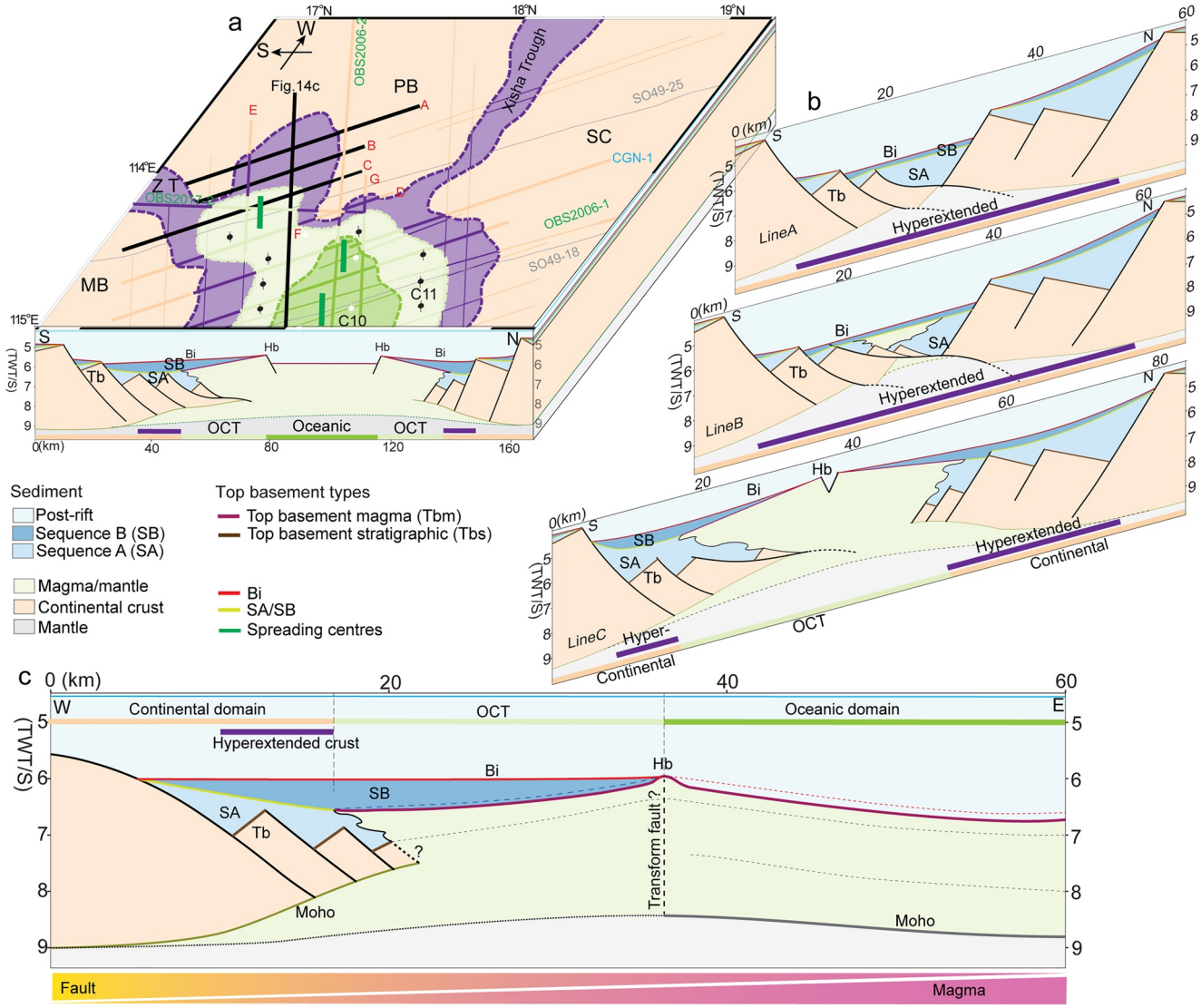

Figure 14. (a) 3D crustal block with the rift domain map. (b) A sequential set of sections across the tip, which correspond to lines A, B and C (see Figures 2–4). (c) A synthetic strike line documenting the transition from the continental domain, including a hyperextended crust, through the ocean continent transition (OCT) domain and to the oceanic domain. Note the link between sedimentary sequences (SA, SB and post-rift) and the location of the domains. SA is syn-hyperextension, SB is syn-breakup (i.e., syn-OCT formation), and the post-rift sequence is syn-seafloor spreading.

6.1. 3D Crustal Architecture at the Tip of the NW-SCS

The 3D crustal architecture of the NW-SCS corresponds, at a plate tectonic scale, to a V-shaped failed oceanic basin that pinches out westwards into rifted crust. At a regional scale the V-shaped basin can be subdivided into a rear, which corresponds to a classical rifted margin with two conjugate margins separated by oceanic crust, and a tip where the ocean pinches out into a severely thinned/hyperextended continental crust, as nicely illustrated in Figures 14a and 14b. Here, we investigate the tip and its relation to the rear and to the rifted crust further to the west.

The 3D crustal block with the rift domain map at its top is displayed in Figure 14a shows the crustal architecture observed at the tip of the NW-SCS. A set of sections documenting the breakup process across the tip are shown in Figure 14b. Figure 14c shows a synthetic strike line documenting the transition from the continental domain, including a hyperextended crust, to an OCT and an oceanic domain. The section also synthesizes the observed relationships between deformation, magmatism, and sedimentation. The sediments of SA seal the faults responsible for hyperextension and interfinger oceanward with magmatic additions. The sediments of SB onlap onto the

Tb of the OCT. The top interface of SB referred to as the breakup interface (Bi), terminates at a basement high (Hb) that delimits the OCT from the first oceanic crust. These relationships, documented in the seismic reflection sections (Figures 2–9) and described in the previous sections, enable a precise temporal and spatial description of the crustal, magmatic and sedimentary evolution at the tip of the NW-SCS during the breakup.

The first-order description is shown in Figure 14 and its interpretation are, however, conflicting with previous interpretations. As shown in Figure 12, C. Li and Song (2012), Y. Li et al. (2021), Zhang et al. (2012) and Cameselle et al. (2017) came to different conclusions and interpretations for the same area. These authors interpreted the tip, imaged by the sections shown in Figure 14b, as the termination of oceanic crust. This interpretation was mainly based on the interpretation of magnetic data, showing a strong positive anomaly (Figure 12c). However, when looking in detail at the seismic reflection sections across the tip, fault-bounded basins with syn-tectonic stratigraphy can be recognized (Figures 2–4). Moreover, sediments belonging to SA can be mapped throughout the tip, always overlying wedging continental crust, and showing syn-tectonic growth structures. The basement underlying SA shows indeed the structural characteristics of continental crust with diagnostic features such as a wedging crust and a Tb offset by faults. More recent and better documented studies tend, however, to put the COB further eastwards. This is nicely documented in Figure 12a, where C. Li and Song (2012) mapped first the COB with the orange line and Zhang et al. (2012) with the light blue line, suggesting that the domain we interpret in our study as the continental domain (Figure 14b) was floored by oceanic crust. Later and based on refraction data, Y. Li et al. (2021) put the COB further eastwards (see red line in Figure 12a). We analyzed the velocity model from Y. Li et al. (2021) (see OBS2017-2; Figure 10b) and compared it with the velocity model from Wu et al. (2012) (OBS2006-1 and OBS2006-2; Figures 11a and 11c). It appears that Y. Li et al. (2021) interpreted our OCT as oceanic crust. Although the definition of OCT may be challenging and difficult to apply, we do not think that the contact between unequivocal continental and oceanic crusts is sharp and can be mapped with a COB (Chao et al., 2021). Our observations show that these two types of crust are separated by a transition zone, which we refer to as the OCT. In the present study, we can see that the OCT has some diagnostic features that can be used for mapping. First, the OCT is overlain by a syn-tectonic sequence (SB) that is never observed over oceanic crust where sediments show passive infill. Another characteristic is the continent-ward tilting of Tb in the OCT domain and the occurrence of an outer high (see Hb in Figure 14c). Moreover, modeling of seismic refraction data generates a transitional velocity structure in the domain we map as an OCT, different from that of both the adjacent continental and oceanic domains. Thus, we consider that mapping a transition (i.e., an OCT) instead of a sharp COB between unequivocal continental and oceanic crusts is more consistent with the observed data and also has major implications for the interpretation of the breakup process.

6.2. Tectono-Magmatic Evolution During Breakup at the Tip of the NW-SCS

Although the observed structures and distribution of magmatic additions and their link to the sedimentary sequences are reasonably well understood along 2D seismic reflection sections (e.g., Figure 14c), it is difficult to understand their relationship in 3D. A key question is how the relatively classical rift structures observed in the rear of the tip terminate and can be linked to the complex rift structures located west of the tip (e.g., Xisha Trough; Figure 14a). Unlike many propagating rifts and oceanic systems showing well defined segments (e.g., see Woodlark Basin; Taylor et al. [2009], the Gulf of California; Lizzaralde et al. [2007], the northern tip of the Red Sea; Ligi et al. [2018], and the Afar/western Gulf of Aden; Nonn et al. [2019]), in the NW-SCS a segmentation is difficult to observe. First-order structural features, such as the trend of magnetic anomalies, a fossil ridge, or the strike of the hyperextended Xisha Trough can be mapped, showing undoubtedly an N-S-directed extension. However, it is difficult to define in detail how these structures terminate and/or to propose transfer zones/faults parallel to the presumed NNW-SSE extension direction. Thus, it remains unclear how the mature oceanic system in the east can be linked to the hyperextended systems in the west, both spatially and temporally. This also questions whether tectonic extension in the west occurred simultaneously with magmatic accretion in the east, in which case this interaction should be observed somewhere in between, spatially and temporally.

An interesting observation, well-illustrated in the crustal domain map (Figure 14a), is the triple junction, where two hyperextended domains join and link with the tip of the NW-SCS, separating three crustal blocks that are the China continental margin in the north, the Macclesfield Bank to the south and the Paracel Bank to the west. Jourdon et al. (2020) successfully reproduced such a structural complexity ahead of a propagator with a numerical model. In their model, the Xisha Trough is presumed to form ahead and simultaneous to the oceanic

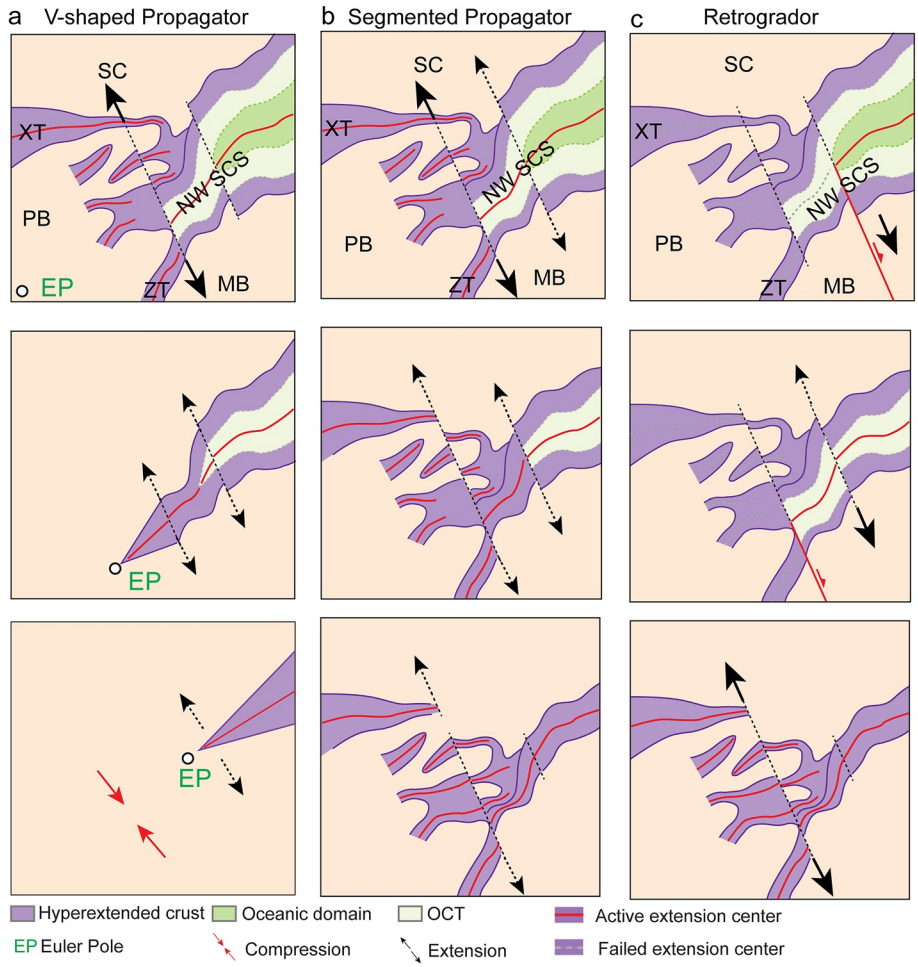

Figure 15. Three kinematic models for the NW-South China Sea, with top row showing present-day rift domain distributions and bottom row showing rift inception for each of the three kinematic models. (Column a) A simple V-shaped propagation without extensional structures ahead of the tip corresponding to the Euler Pole (EP), and compression ahead of the propagator. (Column b) Rift propagation model with widespread hyperextension that occurs simultaneously and ahead of a propagating oceanic system. (Column c) The retrograder model in which the ocean is not propagating into an active rift system, but the whole active rift system is stepping backward while breakup occurs. For explanation and discussion of the models see text.

domain further east (see model in Figure 15b). Our 3D snapshot (Figure 14a) shows a comparable 3D distribution of crustal domains but does not allow for the determination of the origin of this system, hence confirming or rejecting the model of Jourdon et al. (2020). To understand the evolution of the rift system and to evaluate how it propagated, it is important to study the sedimentary architecture along dip and strike lines across the tip of the NW-SCS, since it is the only recorder, apart from the magnetic anomalies, that can help us constrain the temporal evolution of the rift/oceanic system.

In the present study, we defined two sedimentary sequences, SA and SB, and we mapped them across the tip of the NW-SCS, as shown in Figure 13. While SA was deposited during the hyperextension phase, SB was deposited during the OCT formation (for detailed discussion see Sections 4.2 and 5.4). Due to the correlation across the tight network of lines and the relatively small extent of our study area, we are confident that each one of these sequences is isochronous across the study area. This observation implies that the frontal part is not active while the ocean is forming in the rear, in other words that extension stopped in the west, while oceanic accretion continued in the east of the NW-SCS. Thus, we can exclude a propagation model, in which an oceanic domain propagated westward with hyperextension occurring simultaneously further to the west. Instead, our observations suggest that the system was retrograding, that is, when seafloor started in the east, hyperextension has already

ceased in the west. Thus, the rift system did not stall but reorganized. In order to explain this evolution and discuss its consequences for the local and regional geological evolution of the NW-SCS, we propose a conceptual model shown in Figure 15.

6.3. Propagating Versus Retrograding: A New Kinematic Model for the NW-SCS

In Figure 15, we show three imaginable kinematic models for the NW-SCS. Note that the final stage (top panel) is the same for all three models and represents the present-day situation as shown in our rift domain map (Figure 10b). Models shown in Figures 15a and 15b are both propagator models. The first one (Figure 15a) is showing a simple V-shaped propagation without extensional structures ahead of the tip, that would correspond to an Euler pole. Such a model would imply that the domain in front of the propagator, that is, west of the Euler pole is in compression (Martin, 1984). Le Pourhiet et al. (2018) and Luo et al. (2021) showed that such a model is not realistic for the SCS, and more importantly, no compressional structures can be observed in the domain west of the study area (Ding et al., 2012; Gao et al., 2016). In Figure 15b, we show a model in which widespread hyperextension in the west is occurring simultaneously to the propagation of the oceanic system in the east. This model is similar to what has been initially imagined by Vink (1982) and proposed by Taylor et al. (1995) for the Woodlark Basin and by Nierrengarten et al. (2018) for the southern N-Atlantic. It is also in line with what Luo et al. (2021) proposed for the SW-SCS and the models of Le Pourhiet et al. (2018) and Jourdon et al. (2020). This "segmented propagator" model is, however, not compatible with the observations we made in the study area (cf. previous paragraph). Therefore, we propose an alternative model that we refer to as *retrograder* (Figure 15c). In such a model, the ocean is not propagating into an active rift system, but the whole tectonically active system is stepping backward after the continental breakup occurred. Thus, the cessation of rifting and seafloor spreading in the NW-SCS was not due to a stalling of the spreading system but is due to its re-organization. This may be fundamentally different from the SW-SCS, where a stalling of the oceanic spreading system has been documented (e.g., Le Pourhiet et al., 2018; Luo et al., 2021).

The retrograder model (Figure 15c) has major implications for the interpretation of the whole NW-SCS at a regional scale, since it does not only require reassessing the ages of rifting in the different hyperextended basins during early rifting, but also determining and comparing the amount of accommodated extension across sections parallel to the extensional direction through time. It also questions how and where the back-stepping of the rift and spreading system is accommodated since it requires the existence of transfer zones at the terminations of an active segment. Such transfer zones are difficult to determine. One possibility is that the OCT at the tip of the NW-SCS acted as a decoupling zone between the hyperextended systems in the west (e.g., Xisha Trough) and the oceanic domain in the rear. More research is needed to test this hypothesis.

The retrograder model also has more fundamental implications on how plate boundaries form and requires distinguishing between stalling and reorganization of spreading systems, which imply different geodynamic consequences. The model presented here bears some similarities with the ideas proposed by Briais et al. (1993; their figure 17), in which the partitioning between strike-slip movements and complexities in the opening of the SCS are discussed. Our new results lead us to question whether plate boundary formation (i.e., breakup) is controlled by tectonic extension or by magmatic processes. In the example of the SCS, the stalling of the breakup has been explained by gravitational forces (Le Pourhiet et al., 2018), and elsewhere it has been attributed to the occurrence of stronger arc-related rocks (Chenin et al., 2015; Courtillot, 1982). In both cases, failure of the breakup would have a tectonic origin. However, both hypotheses conflict with the observation that the zone ahead of the oceanic crust was dissected by hyperextended basins, suggesting that the strengths/forces were not an obstacle to rifting. An alternative interpretation could be that when the spreading system entered into the former magmatic-arc region, where the mantle is expected to be depleted, magma production was not sufficient to keep seafloor spreading going. A similar interpretation has been proposed to explain magma-poor breakup in the southern N-Atlantic, where it appears that inherited arc settings are not favorable for the breakup, leading to V-shaped basins (e.g., Rockall, Porcupine, Orphan; Chenin et al. [2018]). This interpretation would also explain why the Phu Khanh Basin, which is the only magma-poor rift basin in the SCS where mantle exhumation has been proven (Savva et al., 2014) formed over a former arc domain.

7. Conclusions

Access to a high-resolution seismic reflection dataset from the tip of the NW-SCS enabled us to define and map rift domains and, by comparing them with seismic refraction, magnetic and gravity field data, to define the crustal structure of the OCT. We also analyzed and defined two sedimentary sequences across the tip of the NW-SCS, a first one (SA) deposited during hyperextension and a second one (SB) during the breakup phase/formation of the OCT domain. The combination of the rift domain map with the time constraints obtained from the distribution of SA and SB enabled us to discuss the 3D structural and crustal variability, investigate the extensional and magmatic processes interacting during the breakup, and propose a kinematic evolution for the NW-SCS. The results of this study provide a well-documented example of the spatial and temporal evolution of a rift system during the breakup and show that the V-shaped NW-SCS may not be the result of a stalling oceanic propagator but may rather be explained by the retrogradation and reorganization of a spreading system. Whether the observed evolution can be linked to the inherited arc setting and related depleted mantle, preventing magmatic breakup, needs to be evaluated by future work.

Data Availability Statement

All the data used in this study will be archived in a Figshare repository (https://doi.org/10.6084/m9.figshare.19160801.v4) after acceptance.

Acknowledgments
This manuscript benefited from constructive and careful reviews by Kim Welford and Anne Briais. We thank the editor Jonathan Aitchison for constructive comments and Gwenn Péron-Pinvidic, Laetitia LePourhiet, Manuel Pubellier, Geoffroy Mohn, Daniel Sauter for helpful discussions. This research was financed and supported by the National Natural Science Foundation of China (No.41830537; No.41772109), Key Special Project for Introduced Talents Team of Southern Marine Science and Engineering Guangdong Laboratory (Guangzhou) (GML2019ZD0208), China Scholarship Council (No.201706410090) and supported by the M5/M6 consortium. The authors acknowledge CNOOC for the permission to publish seismic reflection lines.

References

Briais, A., Patriat, P., & Tapponnier, P. (1993). Updated interpretation of magnetic anomalies and seafloor spreading stages in the south China Sea: Implications for the Tertiary tectonics of Southeast Asia. *Journal of Geophysical Research*, *98*(B4), 6299–6328. https://doi.org/10.1029/92JB02280

Cameselle, A. L., Ranero, C. R., & Barckhausen, U. (2020). Understanding the 3d formation of a wide rift: The central south China sea rift system. *Tectonics*, *39*(12), e2019TC006040. https://doi.org/10.1029/2019TC006040

Cameselle, A. L., Ranero, C. R., Franke, D., & Barckhausen, U. (2017). The continent-ocean transition on the northwestern South China Sea. *Basin Research*, *29*, 73–95. https://doi.org/10.1111/bre.12137

Chao, P., Manatschal, G., Chenin, P., Ren, J., Zhang, C., Pang, X., et al. (2021). The tectono-stratigraphic and magmatic evolution of conjugate rifted margins: Insights from the NW south China sea. *Journal of Geodynamics*, 101877. https://doi.org/10.1016/j.jog.2021.101877

Chen, H., Stow, D. A. V., Xie, X., Ren, J., Mao, K., Gao, Y., et al. (2021). Depositional architecture and evolution of basin-floor fan systems since the late Miocene in the northwest sub-basin, south China sea. *Marine and Petroleum Geology*, *126*, 104803. https://doi.org/10.1016/j.marpetgeo.2020.104803

Chenin, P., Manatschal, G., Ghienne, J., & Chao, P. (2021). The syn-rift tectono-stratigraphic record of rifted margins (Part II): A new model to break through the proximal/distal interpretation Frontier. *Basin Research*, *34*(2), 489–532. https://doi.org/10.1111/bre.12628

Chenin, P., Manatschal, G., Lavier, L. L., & Erratt, D. (2015). Assessing the impact of orogenic inheritance on the architecture, timing and magmatic budget of the north Atlantic rift system: A mapping approach. *Journal of the Geological Society*, *172*(6), 711–720. https://doi.org/10.1144/jgs2014-139

Chenin, P., Schmalholz, S. M., Manatschal, G., & Karner, G. D. (2018). Necking of the lithosphere: A reappraisal of basic concepts with thermo-mechanical numerical modeling. *Journal of Geophysical Research: Solid Earth*, *123*(6), 5279–5299. https://doi.org/10.1029/2017JB014155

Courtillot, V. (1982). Propagating rifts and continental breakup. *Tectonics*, *1*(3), 239–250. https://doi.org/10.1029/TC001i003p00239

Ding, W., Schnabel, M., Franke, D., Aiguo, R., & Zhenli, W. (2012). Crustal structure across the northwestern margin of South China sea: Evidence for magma-poor rifting from a wide-angle seismic profile. *Acta Geologica Sinica - English Edition*, *86*(4), 854–866. https://doi.org/10.1111/j.1755-6724.2012.00711.x

Ding, W., Sun, Z., Mohn, G., Nirrengarten, M., Tugend, J., Manatschal, G., & Li, J. (2020). Lateral evolution of the rift-to-drift transition in the South China Sea: Evidence from multi-channel seismic data and IODP Expeditions 367&368 drilling results. *Earth and Planetary Science Letters*, *531*, 115932. https://doi.org/10.1016/j.epsl.2019.115932

Franke, D., Savva, D., Pubellier, M., Steuer, S., Mouly, B., Auxietre, J.-L., et al. (2014). The final rifting evolution in the South China Sea. *Marine and Petroleum Geology*, *58*, 704–720. https://doi.org/10.1016/j.marpetgeo.2013.11.020

Gao, J., Wu, S., McIntosh, K., Mi, L., Liu, Z., & Spence, G. (2016). Crustal structure and extension mode in the northwestern margin of the south China sea: Crustal extension OF the south China sea. *Geochemistry, Geophysics, Geosystems*, *17*(6), 2143–2167. https://doi.org/10.1002/2016GC006247

Gee, J. S., & kent, D. V. (2007). Source of oceanic magnetic anomalies and the geomagnetic polarity time scale. In G. Schubert (ed.), *Treatise on Geophysics*, (Vol. 5, pp. 455–507). Elsevier. https://doi.org/10.7916/D8DV1V8P

Gozzard, S., Kusznir, N., Franke, D., Cullen, A., Reemst, P., & Henstra, G. (2018). South China Sea crustal thickness and oceanic lithosphere distribution from satellite gravity inversion. *Petroleum Geoscience*, *25*(1), 112–128. https://doi.org/10.1144/petgeo2016-162

Hall, R. (1996). Reconstructing Cenozoic SE Asia. In R. Hall, & D. J. Blundell (Eds.), *Tectonic evolution of SE Asia* (pp. 153–184). Geological Society London Special Publication. https://doi.org/10.1144/GSL.SP.1996.106.01.11

Jourdon, A., Le Pourhiet, L., Mouthereau, F., & May, D. (2020). Modes of propagation of continental breakup and associated oblique rift structures. *Journal of Geophysical Research: Solid Earth*, *125*(9), e2020JB019906. https://doi.org/10.1029/2020JB019906

Larsen, H. C., Mohn, G., Nirrengarten, M., Sun, Z., Stock, J., Jian, Z., et al. (2018). Rapid transition from continental breakup to igneous oceanic crust in the South China Sea. *Nature Geoscience*, *11*(10), 782–789. https://doi.org/10.1038/s41561-018-0198-1

Lei, C., Alves, T. M., Ren, J., & Tong, C. (2020). Rift structure and sediment infill of hyperextended continental crust: Insights from 3D seismic and well data (Xisha Trough, South China Sea). *Journal of Geophysical Research: Solid Earth*, *125*(5), e2019JB018610.

Le Pourhiet, L., Chamot-Rooke, N., Delescluse, M., May, D. A., Watremez, L., & Pubellier, M. (2018). Continental break-up of the South China Sea stalled by far-field compression. *Nature Geoscience*, *11*(8), 605–609. https://doi.org/10.1038/s41561-018-0178-5

Le Pourhiet, L., May, D. A., Huille, L., Watremez, L., & Leroy, S. (2017). A genetic link between transform and hyper-extended margins. *Earth and Planetary Science Letters*, *465*, 184–192. https://doi.org/10.1016/j.epsl.2017.02.043

Li, C., & Song, T. (2012). Magnetic recording of the Cenozoic oceanic crustal accretion and evolution of the South China Sea basin. *Chinese Science Bulletin*, *57*(24), 3165–3181. https://doi.org/10.1007/s11434-012-5063-9

Li, C. F., Lin, J., & Kulhanek, D. K. (2015). In International Ocean Discovery Program. *South China sea tectonics* (Vol. 349). *Expedition 349 Scientists*. https://doi.org/10.14379/iodp.proc.349.2015

Li, J., Zhang, Y., Dong, S., & Johnston, S. T. (2014). Cretaceous tectonic evolution of South China: A preliminary synthesis. *Earth-Science Reviews*, *134*, 98–136. https://doi.org/10.1016/j.earscirev.2014.03.008

Li, P. (1993). Cenozoic tectonic movement in the Pearl River Mouth Basin. *China Offshore Oil and Gas*, *7*(6), 11–17.

Li, Y., Huang, H., Grevemeyer, I., Qiu, X., Zhang, H., & Wang, Q. (2021). Crustal structure beneath the Zhongsha Block and the adjacent abyssal basins, South China Sea: New insights into rifting and initiation of seafloor spreading. *Gondwana Research*, *99*, 53–76. https://doi.org/10.1016/j.gr.2021.06.015

Ligi, M., Bonatti, E., Bosworth, W., Cai, Y., Cipriani, A., Palmiotto, C., et al. (2018). Birth of an ocean in the Red Sea: Oceanic-type basaltic melt intrusions precede continental rupture. *Gondwana Research*, *54*, 150–160. https://doi.org/10.1016/j.gr.2017.11.002

Lizarralde, D., Axen, G. J., Brown, H. E., Fletcher, J. M., González-Fernández, A., Harding, A. J., et al. (2007). Variation in styles of rifting in the Gulf of California. *Nature*, *448*(7152), 466–469. https://doi.org/10.1038/nature06035

Luo, P., Manatschal, G., Ren, J., Zhao, Z., Wang, H., & Tong, D. (2021). Tectono - magmatic and stratigraphic evolution of final rifting and breakup: Evidence from the tip of the southwestern propagator in the south China sea. *Marine and Petroleum Geology*, *129*, 105079. https://doi.org/10.1016/j.marpetgeo.2021.105079

Martin, A. K. (1984). Propagating rifts: Crustal extension during continental rifting. *Tectonics*, *3*(6), 611–617.

Neuharth, D., Brune, S., Glerum, A., Heine, C., & Welford, J. K. (2021). formation of continental microplates through rift linkage: Numerical modeling and its application to the flemish cap and Sao Paulo plateau. *Geochemistry, Geophysics, Geosystems*, *22*(4), e2020GC009615. https://doi.org/10.1029/2020GC009615

Nirrengarten, M., Manatschal, G., Tugend, J., Kusznir, N., & Sauter, D. (2018). Kinematic evolution of the southern North Atlantic: Implications for the formation of hyperextended rift systems. *Tectonics*, *37*(1), 89–118. https://doi.org/10.1002/2017TC004495

Nirrengarten, M., Mohn, G., Kusznir, N. J., Sapin, F., Despinois, F., Pubellier, M., et al. (2020). Extension modes and breakup processes of the southeast China-Northwest Palawan conjugate rifted margins. *Marine and Petroleum Geology*, *113*, 104123. https://doi.org/10.1016/j.marpetgeo.2019.104123

Nonn, C., Leroy, S., Lescanne, M., & Castilla, R. (2019). Central Gulf of Aden conjugate margins (Yemen-Somalia): Tectono-sedimentary and magmatism evolution in hybrid-type margins. *Marine and Petroleum Geology*, *105*, 100–123. https://doi.org/10.1016/j.marpetgeo.2018.11.053

Pang, X., Ren, J., Zheng, J., Liu, J., Yu, P., & Liu, B. (2018). Petroleum geology controlled by extensive detachment thinning of continental margin crust: A case study of Baiyun sag in the deep-water area of northern south China sea. *Petroleum Exploration and Development*, *45*(1), 29–42. https://doi.org/10.1016/S1876-3804(18)30003

Pang, X., Zheng, J., Mei, L., Liu, B., Zhang, Z., Wu, Z., & Feng, X. (2021). Structural diversity of fault depressions under the background of preexisting subduction continental margin, Pearl River Mouth Basin, China. *Petroleum Exploration and Development*, *48*(4), 677–687.

Peron-Pinvidic, G., Osmundsen, P. T., & Ebbing, J. (2016). Mismatch of geophysical datasets in distal rifted margin studies. *Terra Nova*, *28*(5), 340–347.

Rowan, M. G. (2018). the South Atlantic and Gulf of Mexico salt basins: Crustal thinning, subsidence and accommodation for salt and presalt strata. *Geological Society, London, Special Publications*, *476*(1), 333–363. https://doi.org/10.1144/SP476.6

Savva, D., Pubellier, M., Franke, D., Chamot-Rooke, N., Meresse, F., Steuer, S., & Auxietre, J. L. (2014). Different expressions of rifting on the South China Sea margins. *Marine and Petroleum Geology*, *58*, 579–598. https://doi.org/10.1016/j.marpetgeo.2014.05.023

Sibuet, J.-C., Yeh, Y.-C., & Lee, C.-S. (2016). Geodynamics of the south China sea. *Tectonophysics*, *692*, 98–119.

Sun, Z., Jian, Z., Stock, J. M., Larsen, H. C., Klaus, A., Alvarez Zarikian, C. A., & Expedition 367/368 Scientists. (Eds.). (2018). *South China sea rifted margin* (Vol. 367/378). *International Ocean Discovery Program*. https://doi.org/10.14379/iodp.proc.367368.2018

Sun, Z., Lin, J., Qiu, N., Jian, Z., Wang, P., Pang, X., et al. (2019). The role of magmatism in the thinning and breakup of the south China sea continental margin: Special topic: The south China sea ocean drilling. *National Science Review*, *6*(5), 871–876. https://doi.org/10.1093/nsr/nwz116

Sun, Z., Zhou, D., Zhong, Z., Xia, B., Qiu, X., Zeng, Z., & Jiang, J. (2006). Research on the dynamics of the South China Sea opening: Evidence from analogue modeling. *Science in China - Series D: Earth Sciences*, *49*(10), 1053. https://doi.org/10.1007/s11430-006-1053-6

Sutra, E., & Manatschal, G. (2012). How does the continental crust thin in a hyperextended rifted margin? Insights from the Iberia margin. *Geology*, *40*(2), 139–142. https://doi.org/10.1130/G32786.1

Taylor, B., Goodliffe, A., & Martinez, F. (2009). Initiation of transform faults at rifted continental margins. *Comptes Rendus Geoscience*, *341*(5), 428–438. https://doi.org/10.1016/j.crte.2008.08.010

Taylor, B., Goodliffe, A., Martinez, F., & Hey, R. (1995). Continental rifting and initial sea-floor spreading in the Woodlark basin. *Nature*, *374*(6522), 534–537. https://doi.org/10.1038/374534a0

Taylor, B., & Hayes, D. E. (1983). Origin and history of the south China sea basin. In *The tectonic and geologic evolution of Southeast Asian seas and Islands: Part 2* (pp. 23–56). American Geophysical Union (AGU). https://doi.org/10.1029/GM027p0023

Tucholke, B. E., Sibuet, J.-C., & Klaus, A. (Eds.), (2007). *Proceedings of The ocean drilling Program, 210 Scientific results*. *Ocean drilling Program* (Vol. 210). https://doi.org/10.2973/odp.proc.sr.210.2007

Tugend, J., Manatschal, G., Kusznir, N. J., Masini, E., Mohn, G., & Thinon, I. (2014). Formation and deformation of hyperextended rift systems: Insights from rift domain mapping in the Bay of Biscay-Pyrenees. *Tectonics*, *33*(7), 1239–1276. https://doi.org/10.1002/2014TC003529

Vink, G. E. (1982). Continental rifting and the implications for plate tectonic reconstructions. *Journal of Geophysical Research*, *87*(B13), 10677–10688. https://doi.org/10.1029/JB087iB13p10677

Wang, Q., Zhao, M., Zhang, H., Zhang, J., He, E., Yuan, Y., & Qiu, X. (2020). Crustal velocity structure of the Northwest Sub-basin of the South China Sea based on seismic data reprocessing. *Science China Earth Sciences*. https://doi.org/10.1007/s11430-020-9654-4

Warner, M. R. (1987). Seismic reflections from the Moho -- The effect of isostasy. *Geophysical Journal International*, *88*(2), 425–435. https://doi.org/10.1111/j.1365-246X.1987.tb06651.x

Wu, Z., Li, J., Ruan, A., Lou, H., Ding, W., Niu, X., & Li, X. (2012). Crustal structure of the northwestern sub-basin, South China Sea: Results from a wide-angle seismic experiment. *Science China Earth Sciences*, *55*(1), 159–172. https://doi.org/10.1007/s11430-011-4324-9

Xie, X., Ren, J., Pang, X., Lei, C., & Chen, H. (2019). Stratigraphic architectures and associated unconformities of Pearl River Mouth basin during rifting and lithospheric breakup of the South China Sea. *Marine Geophysical Research*, *40*(1), 129–144. https://doi.org/10.1007/s11001-019-09378-6

Zhang, C., Su, M., Pang, X., Zheng, J., Liu, B., Sun, Z., & Manatschal, G. (2019). Tectono-sedimentary analysis of the hyper-extended Liwan sag basin (mid-northern margin of the South China Sea). *Tectonics*. https://doi.org/10.1029/2018TC005063

Zhang, C., Sun, Z., Manatschal, G., Pang, X., Li, S., Sauter, D., et al. (2021). Ocean-continent transition architecture and breakup mechanism at the mid-northern South China Sea. *Earth-Science Reviews*, *217*, 103620. https://doi.org/10.1016/j.earscirev.2021.103620

Zhang, C., Sun, Z., Manatschal, G., Pang, X., Qiu, N., Su, M., et al. (2021). Syn-rift magmatic characteristics and evolution at a sediment-rich margin: Insights from high-resolution seismic data from the South China Sea. *Gondwana Research*, *91*, 81–96. https://doi.org/10.1016/j.gr.2020.11.012

Zhang, T., Gao, J., Li, J., Wu, Z., Zhao, L., Yang, C., et al. (2012). The magnetic lineation identifications and segmentation of the northwestern sub-basin in the South China Sea. *Chinese Journal of Geophysics*, *55*(09), 3163–3172. (in Chinese). https://doi.org/10.6038/j.issn.0001-5733.2012.09.034

Zhao, F., Alves, T. M., Xia, S., Li, W., Wang, L., Mi, L., et al. (2020). Along-strike segmentation of the South China Sea margin imposed by inherited pre-rift basement structures. *Earth and Planetary Science Letters*, *530*, 115862. https://doi.org/10.1016/j.epsl.2019.115862

Zhou, D., Ru, K., & Chen, H. (1995). Kinematics of Cenozoic extension on the South China Sea continental margin and its implications for the tectonic evolution of the region. *Tectonophysics*, *251*(1), 161–177. https://doi.org/10.1016/0040-1951(95)00018-6

Zhou, D., Wang, W., Wang, J., Pang, X., Cai, D., & Sun, Z. (2006). Mesozoic subduction-accretion zone in northeastern south China sea inferred from geophysical interpretations. *Science in China, Series A D*, *49*(5), 471–482. https://doi.org/10.1007/s11430-006-0471-9